AD-A096 613 MISSION RESEARCH CORP SANTA BARBARA CA F/G 22/2
ELECTRON SUPPRESSION AND SIMULATION FIDELITY IN THE STRAWMAN DE--ETC(U)
DEC 78 B GOLDSTEIN, J LAVERY, R STETTNER DNA001-78-C-0269
UNCLASSIFIED MRC-R-430 DNA-4755T NL

1 of 1
AD A
096613

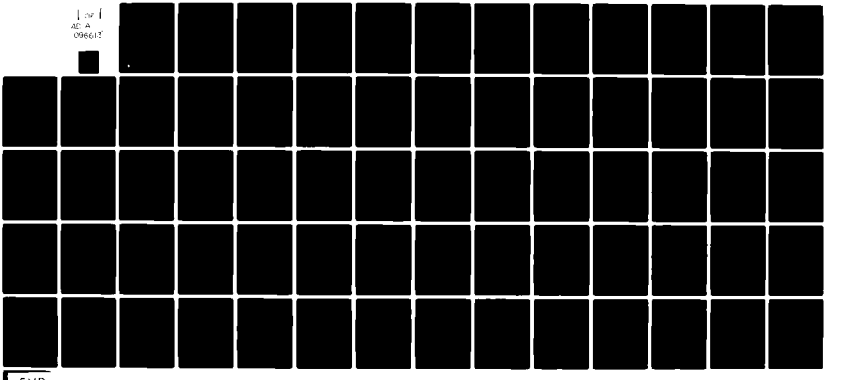

END
DATE FILMED
4 81
DTIC

DNA 4755T

# ELECTRON SUPPRESSION AND SIMULATION FIDELITY IN THE STRAWMAN DESIGN OF SXTF



B. Goldstein
J. Lavery
R. Stettner
Mission Research Corporation
P.O. Drawer 719
Santa Barbara, California 93102

31 December 1978

Topical Report for Period 1 June 1978—31 December 1978

CONTRACT No. DNA 001-78-C-0269



THIS WORK SPONSORED BY THE DEFENSE NUCLEAR AGENCY
UNDER RDT&E RMSS CODE B323078462 G37PAXYX95703 H2590D.

Prepared for
Director
DEFENSE NUCLEAR AGENCY
Washington, D. C. 20305

Destroy this report when it is no longer needed. Do not return to sender.

PLEASE NOTIFY THE DEFENSE NUCLEAR AGENCY, ATTN: STTI, WASHINGTON, D.C. 20305, IF YOUR ADDRESS IS INCORRECT, IF YOU WISH TO BE DELETED FROM THE DISTRIBUTION LIST, OR IF THE ADDRESSEE IS NO LONGER EMPLOYED BY YOUR ORGANIZATION.

UNCLASSIFIED

SECURITY CLASSIFICATION OF THIS PAGE (When Data Entered)

19 REPORT DOCUMENTATION PAGE

READ INSTRUCTIONS BEFORE COMPLETING FORM

| | |
|---|---|
| 1. REPORT NUMBER<br>18 DNA 4755T | 2. GOVT ACCESSION NO<br>AD-A096673 |
| 3. RECIPIENT'S CATALOG NUMBER | |
| 4. TITLE (and Subtitle)<br>(6) ELECTRON SUPPRESSION AND SIMULATION FIDELITY IN THE STRAWMAN DESIGN OF SXTF. | 5. TYPE OF REPORT & PERIOD COVERED<br>9 Topical Report for Period 1 Jun [redacted]—31 Dec 78 |
| | 6. PERFORMING ORG. REPORT NUMBER<br>14 MRC-R-430 |
| 7. AUTHOR(s)<br>(10) B. Goldstein<br>J. Lavery<br>R. Stettner | 8. CONTRACT OR GRANT NUMBER(s)<br>13 DNA 001-78-C-0269 |
| 9. PERFORMING ORGANIZATION NAME AND ADDRESS<br>Mission Research Corporation<br>P.O. Drawer 719<br>Santa Barbara, California 93102<br>17 X957 | 10. PROGRAM ELEMENT, PROJECT, TASK AREA & WORK UNIT NUMBERS<br>16 Subtask G37PAXYX957-03 |
| 11. CONTROLLING OFFICE NAME AND ADDRESS<br>Director<br>Defense Nuclear Agency<br>Washington, D.C. 20305 | 12. REPORT DATE<br>11 31 Dec [redacted]978<br>13. NUMBER OF PAGES<br>12 68 |
| 14. MONITORING AGENCY NAME & ADDRESS (if different from Controlling Office) | 15. SECURITY CLASS. (of this report)<br>UNCLASSIFIED |
| | 15a. DECLASSIFICATION/DOWNGRADING SCHEDULE<br>N/A |

16. DISTRIBUTION STATEMENT (of this Report)

Approved for public release; distribution unlimited.

17. DISTRIBUTION STATEMENT (of the abstract entered in Block 20, if different from Report)

18. SUPPLEMENTARY NOTES

This work sponsored by the Defense Nuclear Agency under RDT&E RMSS Code B323078462 G37PAXYX95703 H2590D.

19. KEY WORDS (Continue on reverse side if necessary and identify by block number)

SGEMP Simulation
Simulation Quality
Tank Physics

20. ABSTRACT (Continue on reverse side if necessary and identify by block number)

This report discusses the quality of SGEMP simulation which would exist in the Satellite X-ray Test Facility if it were constructed in accordance with the proposed strawman design.

It was found that the simulation quality at some locations on a test satellite is poor, suggesting that a modification of the strawman design may be necessary.

DD FORM 1 JAN 73 1473 EDITION OF 1 NOV 65 IS OBSOLETE

UNCLASSIFIED 406548 JLL

SECURITY CLASSIFICATION OF THIS PAGE (When Data Entered)

# PREFACE

The authors would like to express their sincere thanks to four individuals who greatly assisted in the course of this work. We thank Mr. Robert Marks for his valuable assistance with the computational aspects of this work. Dr. Neal Carron and Dr. William Crevier have contributed their expertise on certain aspects of SXTF design and numerical techniques. Finally, we wish to acknowledge Mr. Steve Schwartz for calculating the electron emission spectra.

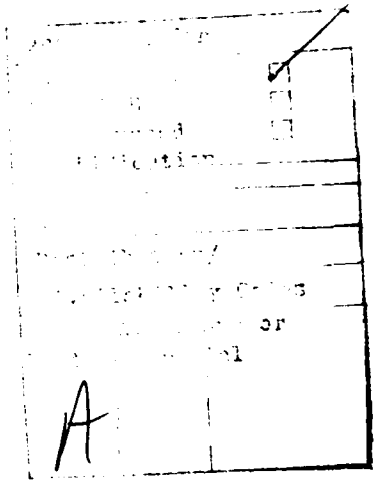

TABLE OF CONTENTS

## LIST OF ILLUSTRATIONS

LIST OF ILLUSTRATIONS (cont'd)

# SECTION 1
# INTRODUCTION

It is the purpose of this report to present the results of a recent investigation into the quality of SGEMP simulation which can be expected in the proposed Satellite X-ray Test Facility. The strawman design which will be criticized in this report consists of a spherical vacuum tank 30 m in diameter with a concentric, transparent, non-emitting damper membrane whose diameter is 80 percent of the tank's diameter.[1] The X-ray illumination is caused by both a compact exploding wire and an extended bremsstrahlung source. In this study, we wish to determine how closely the SGEMP response of a test body placed in this simulator corresponds with the response of the same body in free space.

In order to examine the simulation quantitatively, we compare the results of code calculations of the SGEMP response of a test body placed in the tank to that of the same body in free space. Several potentially important effects are introduced by the tank. First, electromagnetic energy cannot be radiated into free space but is instead reflected from the tank walls and returned to the test object. These reflections cause the deposition of additional electromagnetic energy in the satellite possibly causing severe overtesting and even satellite damage. In an effort to overcome this difficulty the resistive membrane is placed inside the tank. An additional complication is caused by the emission of electrons from the tank walls. These particles are a source of unwanted electromagnetic fields and can also charge the test object.

In order to isolate each of these effects we have performed calculations in which no electron emission occurs from the walls or from the membrane. This calculation simulates perfect suppression of wall and membrane emission. It demonstrates the effects of reflection from the tank walls and absorption of energy by the resistive membrane. We then examine the quality of simulation provided by the strawman design in which electron emission from the tank is included. Finally, we examine the extreme case of an emitting membrane and emitting wall. Some damper designs have proposed the use of sheets of conducting low $\Sigma$ material rather than ohmic meshes and in this calculation we study the effects of membrane emission. Although this calculation may not prove to be relevant to the SXTF design, it is reported here since it may be of interest in connection with other SGEMP experiments.

It is the aim of these studies to determine whether the passive suppression provided by the low $\Sigma$ emission from the walls of the tank is adequate or whether active suppression is required.

Since the SXTF may, at some future date, be used to test satellites whose dimensions are comparable to the dimensions of the tank, we wish to determine to what extent the SGEMP is affected when parts of the satellite are in close proximity to the tank walls and to the membrane.

In Section 2 we describe our method of calculation and discuss the various approximations and assumptions made. A detailed presentation of the results of our calculations is provided in Section 3. Section 4 is devoted to a discussion of the significance of our results and in Section 5 we make our recommendations for modifications of the strawman design.

# SECTION 2
# METHOD OF CALCULATION

Our calculations were performed using the two-dimensional cylindrically symmetric particle pushing code SEMP, a detailed account of which is provided in Reference 2. Several important modifications to this code were required for our tank simulations and we shall discuss these modifications in this section.

## 2.1 CODE DESCRIPTION OF THE SXTF

The tank simulator is sketched in Figure 1. Basically, it consists of a spherical vacuum tank (stainless steel) 15 m in radius from which a segment has been removed in order to provide a suitable location for the radiation sources. The total length of the assembly is thus 24 m. In SEMP, this is represented by a grid of 133 × 83 cells each 18 cm in the radial and axial directions. A resistive membrane, spherical in shape and of radius 12 meters is positioned concentric with the sphere and the satellite was placed inside the membrane.

## 2.2 MESH AND BOUNDARY CONDITIONS

As with any finite difference scheme, our mesh must be small enough to provide an adequate description of the phenomenon of interest, in our case the motion of the electrons and the fields so produced, yet large enough so that calculation does not become excessively time consuming or require unduly large amounts of core. The mesh size determines the time step because of the requirement that Courant's condition be satisfied.

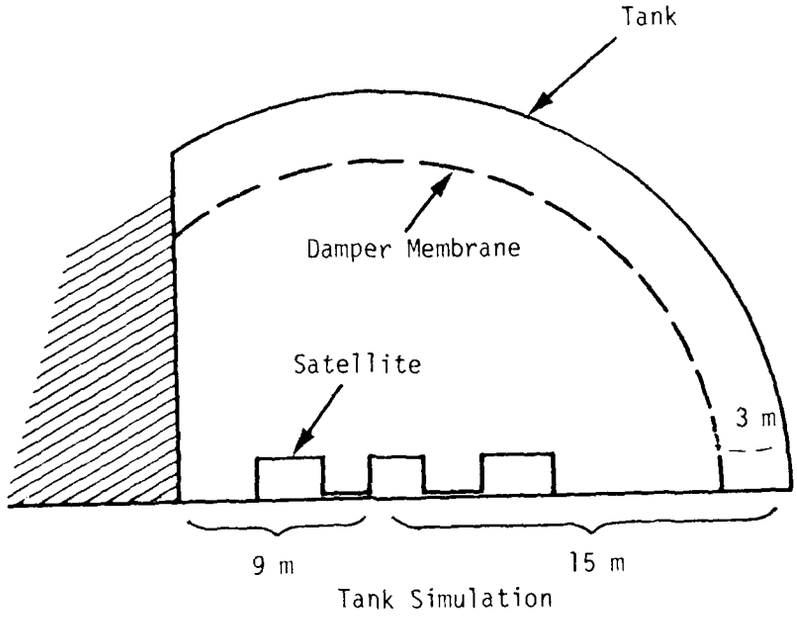


Figure 1. Schematic drawing of SXTF. The membrane is 3 m from the tank walls.

We therefore require as large a mesh as possible consistent with accurate representation of the motion of charge.

The original SEMP mesh[2] used three interlocking meshes with the body drawn in the smallest mesh and the outer boundary in the largest mesh. Our free space calculations used the three meshes and the transmitting outer boundary condition. In our tank calculations, however, we have a reflecting and emitting outer boundary, the walls of the tank. Accurate representation of the emission of particles from the tank walls demands that the mesh spacing at the outer boundary be smaller than the Debye length in the charge cloud. Satisfaction of this condition precludes the use of the three mesh system and a single uniform mesh was used.

A sphere was drawn inside this mesh. The usual boundary conditions were applied at the surface of the sphere. The walls of the tank are assumed to be infinitely conducting so that the tangential component of the electric field must vanish at its surface. The reflecting boundary condition is also applied here.

The mesh spacing in these calculations was uniform with $\Delta r = \Delta z = 18$ cm. Under conditions of extreme space-charge-limiting, this mesh is inadequate since the Debye length is smaller than the mesh spacing ($\lambda_D \sim 1$ cm). This condition prevails at the emitting surface of the satellite but not at the tank walls ($\lambda_D \sim 20$ cm). At the emitting surface of the satellite, particle motion cannot be described in this mesh and we must use an alternative description of the currents at that position. In a space-charge-limited situation, a dipole layer forms above an emitting surface. The current density may be described in terms of the time derivative of the dipole moment per unit area. A $\dot{P}$ driver may be calculated for a given X-ray spectrum and time history for a given material using the one-dimensional particle pushing code SCALID, details of which may be found in Reference 3.

In the SXTF strawman design, two sources of radiation are used—a compact exploding wire source and a more extended bremsstrahlung source. Since the bremsstrahlung spectrum is considerably harder than the exploding wire spectrum (2 keV blackbody), fewer electrons are produced so that the Debye length in the charge cloud produced by the bremsstrahlung is larger than the cell size. For this reason, a dipole driver description of the bremsstrahlung excitation is unnecessary, although it is required to simulate the boundary layer associated with the exploding wire photon source.

## 2.3 OTHER CODE MODIFICATIONS

In the SEMP code, particles inside a particular cell are moved using interpolated values of the electric and magnetic fields. The interpolation is linear using the field values at the corners of the cell. If one has a conductor (e.g., the damping membrane) embedded in the mesh, the fields are discontinuous at its surface. Under these circumstances, a reliable estimate of the field at a particular point can no longer be obtained by interpolation and we use the nearest grid point method. In this method, particles are moved using the values of the fields at the grid point closest to the particle, on the same side of the conductor. One thus avoids the difficulty of interpolating across a discontinuity.

In our calculations, we have represented a spherical surface in a cylindrical mesh. The cylindrical mesh was chosen as a matter of convenience since the satellite is more easily represented in a cylindrical mesh. This representation of a spherical surface can lead to inaccuracies in the rate of propagation of fields if the wall of the tank passes diagonally through a cell. Consider the cell shown in Figure 2 through which the tank wall passes diagonally. A signal propagating from A to B reaches B in a time $\sqrt{2}\Delta\lambda/c$. In the code calculations, such a signal would be required to travel through C, reaching B in a time $2\Delta r/c$.

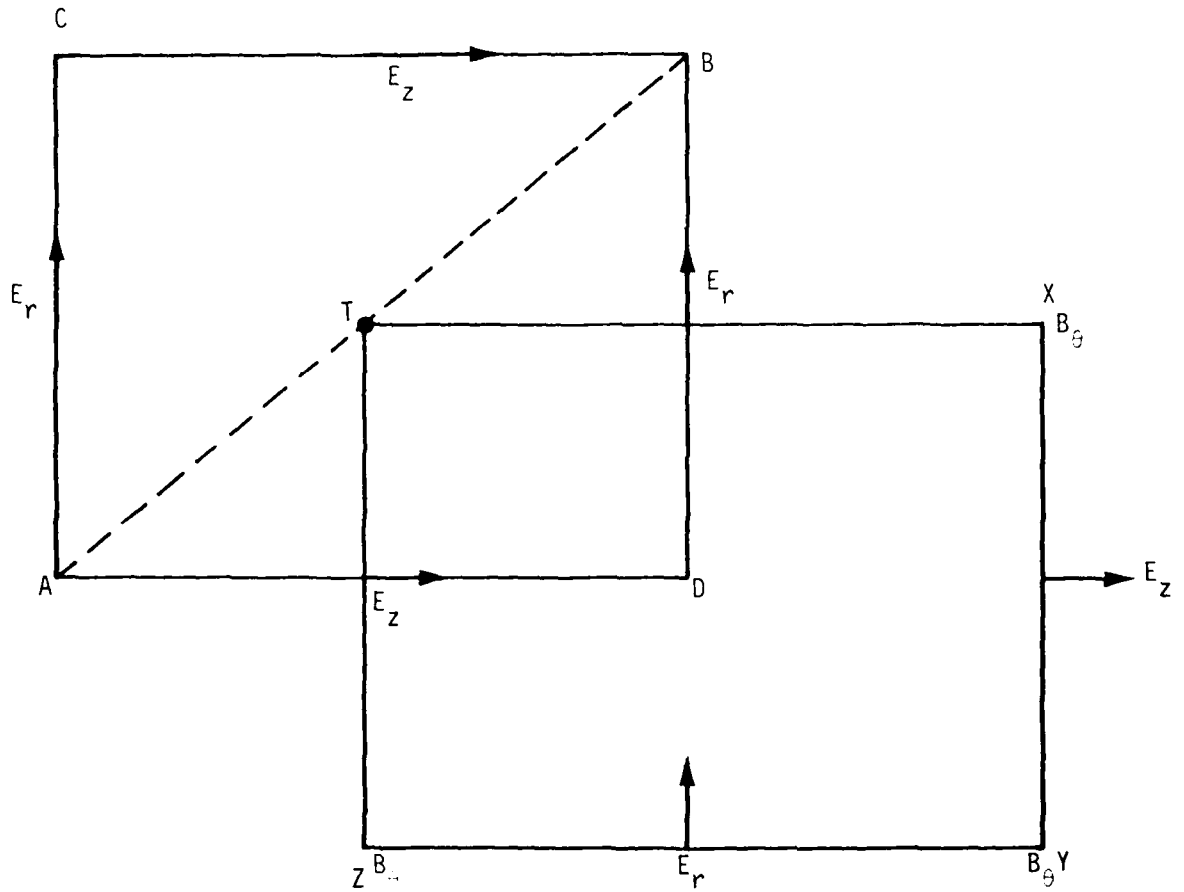


Figure 2. Part of the mesh in the vicinity of the tank wall. The wall coincides with AB.

In order to correct this inaccuracy, we proceed as follows. Faraday's equation may be written

$$\frac{\partial}{\partial t}\int_{\text{cell}} \underset{\sim}{B}\cdot d\underset{\sim}{a} = -c\int \underset{\sim}{E}\cdot d\underset{\sim}{\ell}\ .$$

In any ordinary cell of the mesh, we can write the integral on the left as

$$\frac{\partial}{\partial t}\ (\Delta r\Delta z)B\ ,$$

but when the tank wall passes diagonally through a cell, the integral is over a half cell and we have

$$\frac{\partial}{\partial t}\int_{ADB} \underset{\sim}{B}\cdot d\underset{\sim}{a} = \frac{\partial}{\partial t}\left(\frac{\Delta r\Delta z}{2}\right)\underset{\sim}{B}\ .$$

Using Stoke's theorem, we have

$$\frac{1}{2}\frac{\partial}{\partial t}\int \underset{\sim}{B}\cdot d\underset{\sim}{a} = -c\int \underset{\sim}{\nabla}\times\underset{\sim}{E}\cdot d\underset{\sim}{a}\ .$$

Removing the integration signs, we obtain

$$\frac{1}{2}\frac{\partial \underset{\sim}{B}}{\partial t} = -c\underset{\sim}{\nabla}\times\underset{\sim}{E}\ .$$

Amperes law may be written

$$4\pi\int_{TXYZ}\underset{\sim}{J}\cdot d\underset{\sim}{a} + \frac{1}{c}\frac{\partial}{\partial t}\int_{TXYZ}\underset{\sim}{E}\cdot d\underset{\sim}{a} = \int \underset{\sim}{B}\cdot d\underset{\sim}{\ell}\ .$$

Using Stoke's theorem and removing the integration sign we find that

$$\underset{\sim}{\nabla}\times\underset{\sim}{B} = 4\pi\underset{\sim}{J} + \frac{1}{c}\frac{\partial \underset{\sim}{E}}{\partial t}\ .$$

Since the integration is over the cell TXYZ, Ampere's equation is unchanged.

Combining Ampere's and Faraday's equations, we have

$$\underset{\sim}{\nabla} \times \underset{\sim}{\nabla} \times \underset{\sim}{E} = - \frac{1}{2c} \frac{\partial}{\partial t} \left(4\pi \underset{\sim}{J} + \frac{1}{c} \frac{\partial \underset{\sim}{E}}{\partial t}\right) .$$

In vacuum, we have

$$\nabla^2 E = \frac{1}{2c} \frac{\partial^2 E}{\partial t^2} .$$

This is a wave equation with effective propagation velocity $\sqrt{2}c$. The introduction of the factor of 2 in Faraday's equation corrects the propagation velocity in those cells through which the tank wall passes diagonally. In all other cells this correction is unnecessary.

## 2.4 RETARDATION OF THE RADIATION PULSE

Since the duration of the X-ray pulse from both the exploding wire source and the bremsstrahlung source is shorter than the light travel time across the tank, care must be taken to retard the emission from a point by the appropriate light travel time. The zero point of time occurs when the first emission point (either on the satellite or on the wall of the tank) starts to emit. The first emission point is the emission point closest to the radiation source. Let its $\Xi$ coordinate be denoted by $\Xi_0$. A point at $\Xi_1$ will not begin to emit until the pulse has reached it, i.e., at time $\Xi_1 - \Xi_0/c$. Every emission point emits with some pulse time history. However, the pulse at each point is displaced by the amount $(\Xi - \Xi_0)/c$.

The X-ray pulse is thus treated as a plane wave propagating in the $\Xi$ direction; the time of emission from a point is determined by its $\Xi$ coordinate. The plane wave approximation is appropriate when we are considering the extended bremsstrahlung source but may be slightly in error when we are considering the more compact exploding wire source which is better represented by a spherical wave.

## 2.5 DAMPING MEMBRANE

The membrane serves two purposes. In all SXTF calculations, the membrane extracts energy from the wave reflected from the tank walls. Its purpose is to diminish the effect of reflection so that the tank more closely simulates free space. In some calculations, we examined a non-transparent membrane which emits electrons and through which particles cannot pass. In these calculations, the membrane has the additional functions of electron emitter and absorber.

The resistive membrane is simulated by assigning a resistance to those cells which correspond to the position of the membrane. It has been shown[4] that the optimal membrane impedance is $Z = Z_0/2$ where $Z_0$ is the impedance of free space 378 Ω. Since the behavior of the fields is not very sensitive to the value of the impedance, we chose a value of 200 Ω/square. We then reduced the electric field components by a factor of $1/(1 + Z_0 c\Delta t/Z\Lambda)$ where c is the speed of light and $\Delta t$ and $\Lambda$ are the time step and spatial size respectively.[4] This procedure removes energy from the tank in order to produce a better simulation of free space.

## 2.6 THE TEST SATELLITE

The satellite chosen for our simulation test was a FLTSATCOM like the model, a rough sketch of which is shown in Figure 3a. This choice was made since it is of interest to examine the response of a resonant body. It may stress the simulation fidelity requirement to a greater extent than a non-resonant body because it has characteristic frequencies which persist in time.

Our satellite model shown in Figure 3b consists of three cylinders each of length 2 m and radius 1 m connected by thin struts 2.5 cm in diameter. Since the struts cannot be properly described in this mesh, a

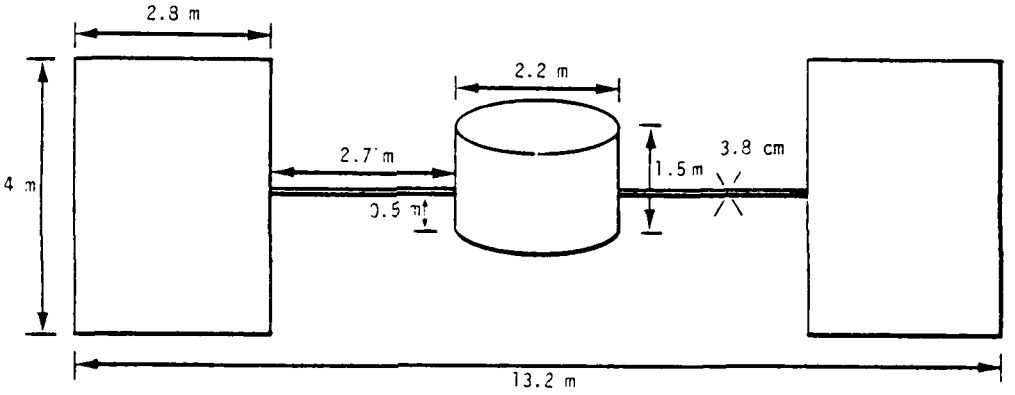


Figure 3a. Schematic drawing of FLTSATCOM.

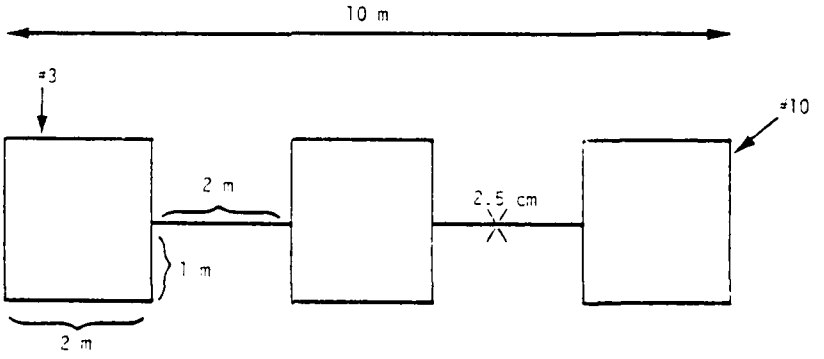


Figure 3b. Satellite.

Figure 3. Model satellite used in code.

special treatment was necessary. Our treatment of struts is outlined in Appendix A.

## 2.7 PARAMETERS OF THE CALCULATIONS

We now give the numerical values of the various quantities used in our calculations.

All calculations presented in Section 3 assume an X-ray fluence of $5 \times 10^{-4}$ cal/cm$^2$/sec. The X-ray flux has two distinct components—a bremsstrahlung component and an exploding wire component. The bremsstrahlung component has an essentially flat spectrum as shown in Figure 4a and a triangular time history which peaks in 15 ns and falls slowly to zero at 70 ns (Figure 4b). The exploding wire spectrum is that of a 2 keV black body and its time history is somewhat complicated (Figure 4c). A peak of the exploding wire radiation occurs after only 7.5 ns and is followed by a rapid decline. This initial peak is followed by several secondary peaks. Because of Debye length considerations discussed previously, exploding wire radiation is represented at the surface of the satellite by the $\dot{P}$ driver shown in Figure 4d.

The energy spectrum of electrons emitted from the satellite was taken to be the backward emitted spectrum for aluminum. Emission from the tank assumes the forward emitted spectrum of carbon. Use of the forward spectrum is not strictly correct but comparison of the forward and backward spectra of carbon shows that the error introduced is small. Although the photoelectric yield of carbon is smaller than that of aluminum, the walls of the tank have a much larger area than the satellite and consequently emit approximately an order of magnitude more electrons.

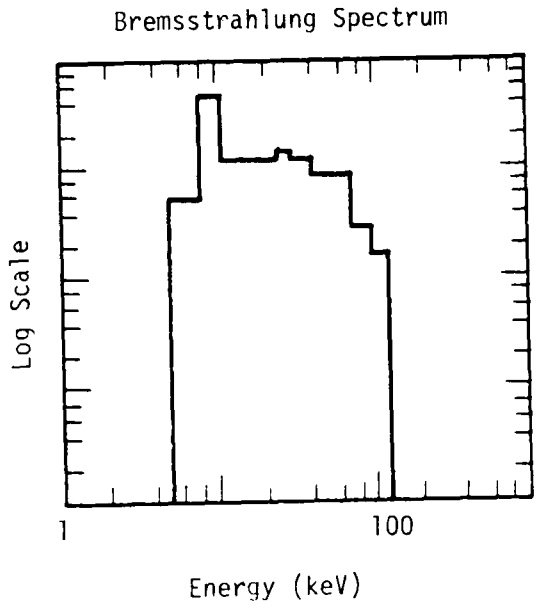


4a.

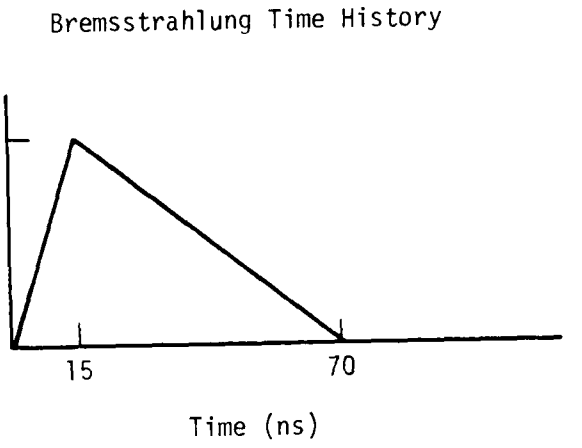


4b.

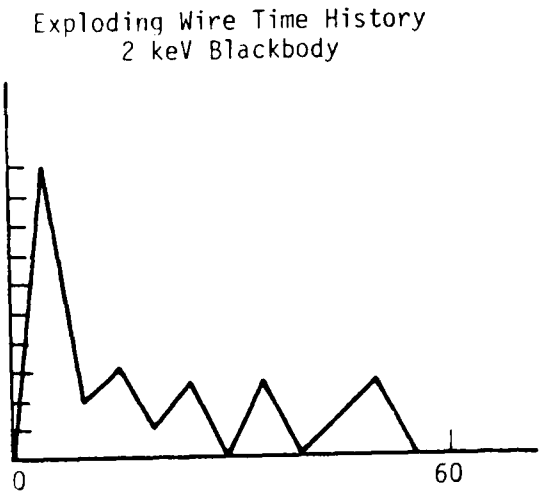


4c.

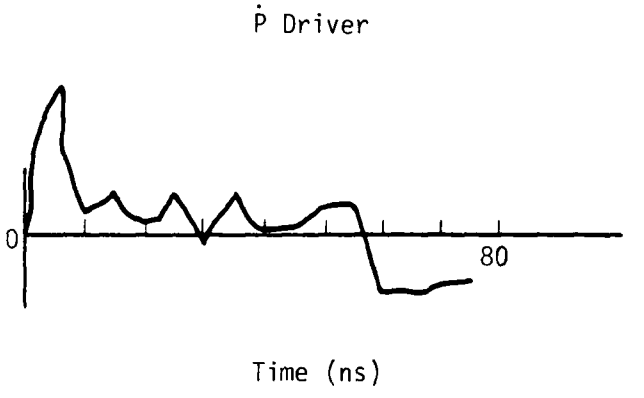


4d.

Figure 4. Spectra and time histories of X-ray drivers.

# SECTION 3
# RESULTS OF THE CALCULATIONS

The present section is the first of two devoted to a detailed presentation and discussion of the results of our calculations. A brief summary of the initial assumptions of the various runs is given in Table 1.

## 3.1 SATELLITE IN FREE SPACE

Since in a perfect simulator, the SGEMP response of a body inside a test tank should be the same as that of the same body in free space, it is useful for comparison purposes to calculate the free space response of our test body.

In the free space run, the outer boundary condition is such as to allow essentially all of the electromagnetic energy reaching the outer boundary to be radiated. The treatment of the outer boundary condition introduces a fractional error of approximately $\lambda/2\pi R$ (see Reference 5), where $\lambda$ denotes the longest wavelength of electromagnetic radiation of interest (which is of the order of the length of the satellite) and R is the radial distance to the outer boundary. For accuracy, it is required that the fraction $\lambda/2\pi R$ be small compared to unity. This condition requires that the distance to the outer boundary be much larger than the dimensions of the test body. Computer storage limitations make it difficult to satisfy this requirement while providing a sufficient number of cells for an accurate description of the satellite. To satisfy this requirement while keeping computational demands at a reasonable level, we made use of the three

Table 1. Summary of cases discussed in Section 3.

| | Tank Present | Perfect Suppression | Emitting Membrane | Absorbing Membrane | Membrane Damping | Satellite Off Center | |
|---|---|---|---|---|---|---|---|
| 1 | | | | | | | Free Space |
| 2 | X | X | | | X | | Centered Perfect Suppression |
| 3 | X | | | | X | | Centered Strawman |
| 4 | X | | X | X | X | | Centered Emitting Membrane |
| 5 | X | X | | | X | X | Shifted Perfect Suppression |
| 6 | X | | | | X | X | Shifted Strawman |
| 7 | X | | X | X | X | X | Shifted Satellite and Emitting Membrane |

interlocking meshes of increasing size of the original SEMP code rather than using the single mesh.

In a perfect SGEMP simulator, the fields should be identical to those calculated for the free-space case being free from reflected signal and oscillations resulting from the excitation of the natural modes of the tank.

An additional effect is introduced by the presence of the tank. Although the walls of the tank are coated with carbon, a material of low Z and low photoelectric yield, the tank has a much larger surface area than the satellite and emits considerably more electrons. The irradiation of the tank and satellite by X rays produces a larger quantity of electromagnetic energy than was produced by the irradiation of the satellite in free space and it is of interest to examine the effects of this additional energy.

## 3.2 OVERVIEW OF THE CALCULATIONS

In order to examine quantitatively the effects of reflection and photoelectric emission from the tank, three other cases have been calculated.

### Case A—Perfect Suppression

In this case, no emission takes place either from the walls of the satellite or from the membrane. The only emitting surface in the problem is the front surface of the satellite. We call this case perfect suppression because the electron emission from the tank walls are completely suppressed.

The assumption of a non-emitting tank is not physically justifiable but the calculation is intended to model perfect suppression of electron emission from the tank walls and isolate the effects of reflection from the tank.

### Case B—Strawman

In this case, we model the strawman design for the SXTF described in Reference 1. The satellite is placed inside a vacuum tank whose walls are coated with carbon. Emission takes place from the walls with the photoelectric yield appropriate to carbon. The damper membrane is described in Reference 1 as an ohmic mesh made up of carbon coated fiberglass 0.5 cm in diameter made into a mesh with 10 cm spacing. In the calculations we assign the appropriate resistance to the membrane, 200 Ω/square, and assume that it is non-emitting and transparent in the sense that electrons pass freely through it.

This calculation is intended to be physically realistic and is designed to isolate the potentially important effects of electron emission from the walls.

### Case C—Emitting Walls and Membrane

Since other designs of damper membranes have been considered for the SXTF, we examine the case where a non-transparent, emitting carbon membrane is used. In this case, electrons are not allowed to pass freely through the membrane but are absorbed upon reaching it. The membrane also emits from both sides with the photoelectric yield of carbon.

Cases A-C were calculated with the satellite centered and again with the satellite close to the emitting membrane. The latter (shifted) configuration was designed to test the situation in which a part of the satellite was close to an emitting surface.

## 3.3 OVERVIEW OF THE RESULTS

A useful measure of the Joule heating of electronic circuitry due to an induced electromotive force is the quantity $\int B^2(t)dt$. Comparison of this quantity for various cases provides an indication of the simulation fidelity. We are also interested in the behavior of the skin current and normal components of the electric fields at various points on and near the surface of the satellite.

In this report all electric fields are expressed in statvolts per centimeter. Skin currents are reported in Amperes per meter. The time integral of the square of the magnetic field is always given in arbitrary units.

The fields are calculated and plotted for ten points but here we present the results for two representative points. Observer point 3 (see Figure 3) is close to the emitting surface of the satellite. Observer point 10 is on the surface farthest from the radiation source. The signal at point 3 is dominated by the emission from the front face of the satellite. At point 10, the effects of reflected signals and electron emission from the tank are much more readily seen. Our main results may be summarized as follows.

The simulation fidelity is adequate at point 3 satisfying the fidelity criteria described in Reference 6. Departures from the free space response occur in both the strawman and emitting membrane cases. The electric field at point 10 at late time is dominated by a tank induced pulse which is stronger than the initial pulse. Considerably more energy is deposited at observer point 10 in the strawman and emitting membrane cases than in the free space case. At observer 10, the unshifted satellite strawman case fails to satisfy the criteria for adequate simulation fidelity.

In the case where the satellite is positioned off center, the departure from the free-space response is more severe. Simulation fidelity is still adequate at observer point 3 but at point 10 dramatic differences

appear. The behavior of the electric field at point 10 is characterized by a large negative spike occurring at the time of reflection. The spike is an order of magnitude greater than the initial spike in the free space case. The integral of $B^2$ is greater than in the free space case by a factor of 200. The simulation fidelity at point 10 in the shifted satellite case must be considered inadequate.

We do not consider that an overtest has occurred since the fields at point 10 in the strawman case are comparable to those at point 3 for the free space case. However, the fields at point 10 are not faithfully reproduced by the simulator.

## 3.4 SIMULATION QUALITY FOR CENTERED SATELLITE CASE

We now present the results of our test simulations and discuss in detail the quality of simulation paying particular attention to the causes of the departures of the SGEMP response from the free-space response. We first examine those test simulations in which the satellite was centered in the tank.

In Figure 5, we compare the integral of $B^2$ for all four cases at observer point 3. The general behavior of the integral is similar in all cases rising rapidly from zero and flattening off at late time. Slight differences appear in the perfect suppression and strawman cases and slightly higher ($\sim$ 20 percent) values of the integral are attained. This indicates that reflection from the tank walls causes the deposition of additional energy at observer point 3. The differences between Figures 5b and 5c are attributable to electron emission from the walls of the tank. Reflection from the tank walls produces a slight $\sim$ 10 percent increase in the maximum value of $\int B^2(t)dt$ and electron emission produces a further 20 percent increase. As one would expect, the early parts of the curves are almost identical with the differences occurring at late time $t > 100$ ns. These figures indicate that noticeably larger amounts of energy are deposited at observer point 3 in the tank simulation cases than in the free space case, but the

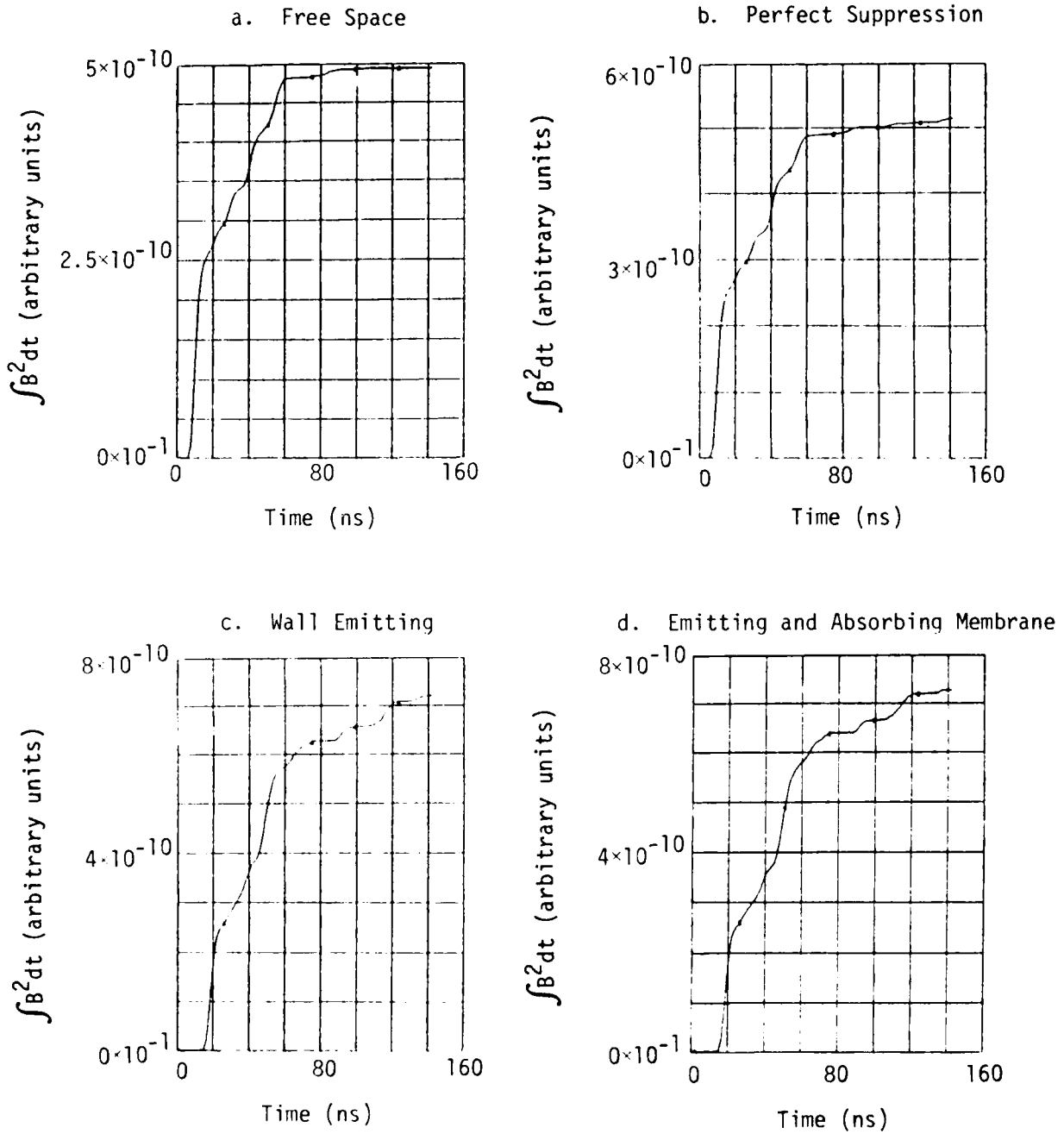


Figure 5. Integral of $B^2(t)$ observer point 3 (unshifted).

effects of reflection and emission from the tank walls do not appear to be serious at observer point 3.

The integral is plotted in Figure 5d for the case in which the membrane emits and absorbs electrons. Comparison of Figure 5c and 5d indicates that the absorption and emission of electrons by the damper membrane has no major effect on the quantity of energy deposited at this observer point.

We now examine the fields and currents produced in these tests. Figure 6 shows the skin current at observer 3. Little difference is seen between the various cases at point 3; each shows a large initial spike, followed by subsequent oscillations. In the free-space case, the skin current had returned to zero by 100 ns whereas oscillations continued at late time when the satellite was placed inside the vacuum tank. The straw-man and emitting membrane cases reveal that the late-time oscillations are stronger when more electrons are present (compare Figure 6b with Figures 6c and d).

Figure 7 shows the behavior of the normal component of the electric field at observer point 3. The changes in the normal component of the electric field at observer 3 resulting from reflection or emission from the tank are very small at observer point 3.

From the results shown in Figures 5 through 7, we must conclude that the quality of simulation at observer point 3 in the centered satellite cases is very good. Because observer point 3 is close to the emitting surface, the magnitude of the reflected pulse is small compared to the initial pulse. It is for this reason that little difference is seen between the free-space case and the case in which the satellite is enclosed in the tank.

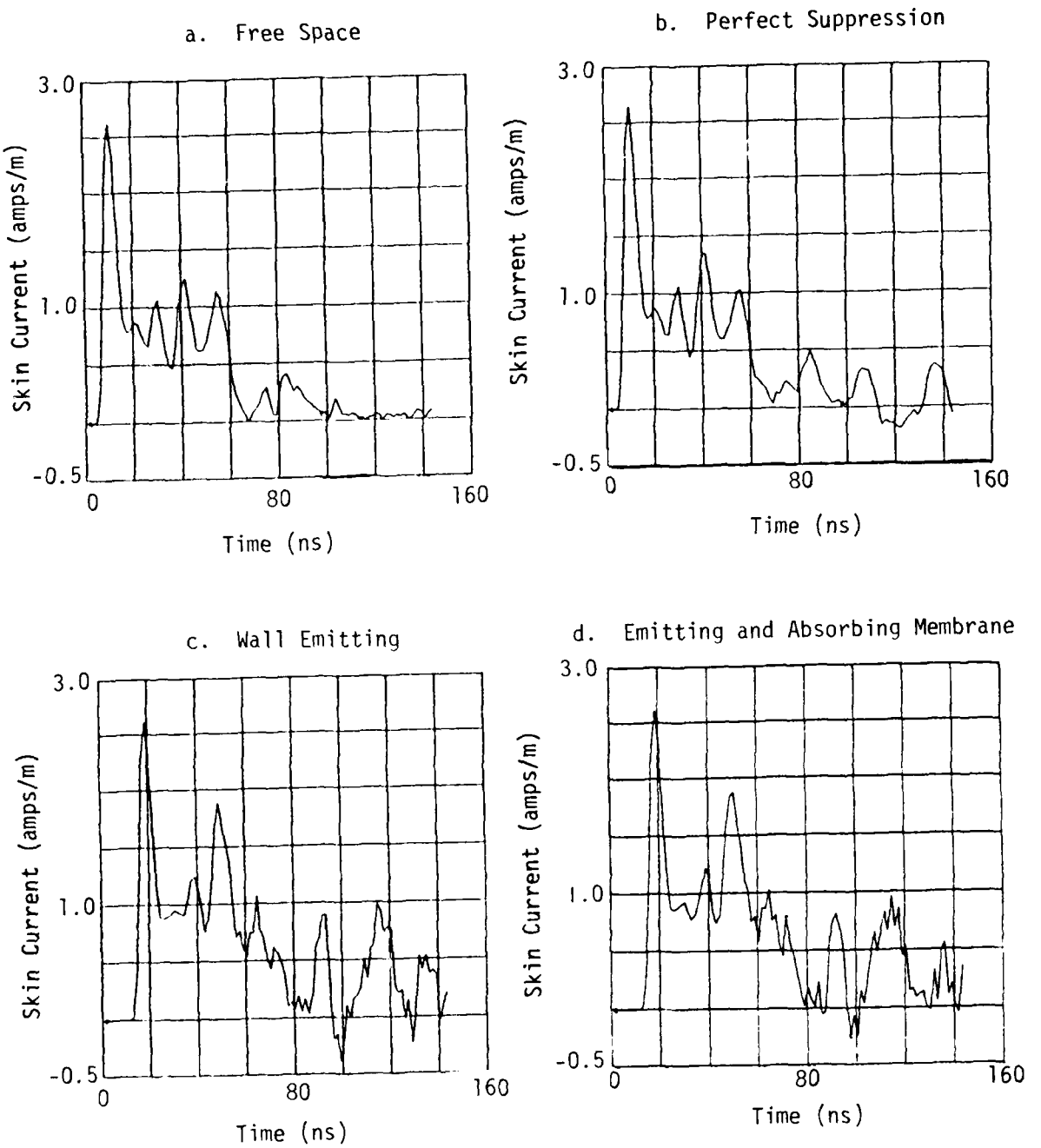


Figure 6. Skin current observer point 3 (unshifted).

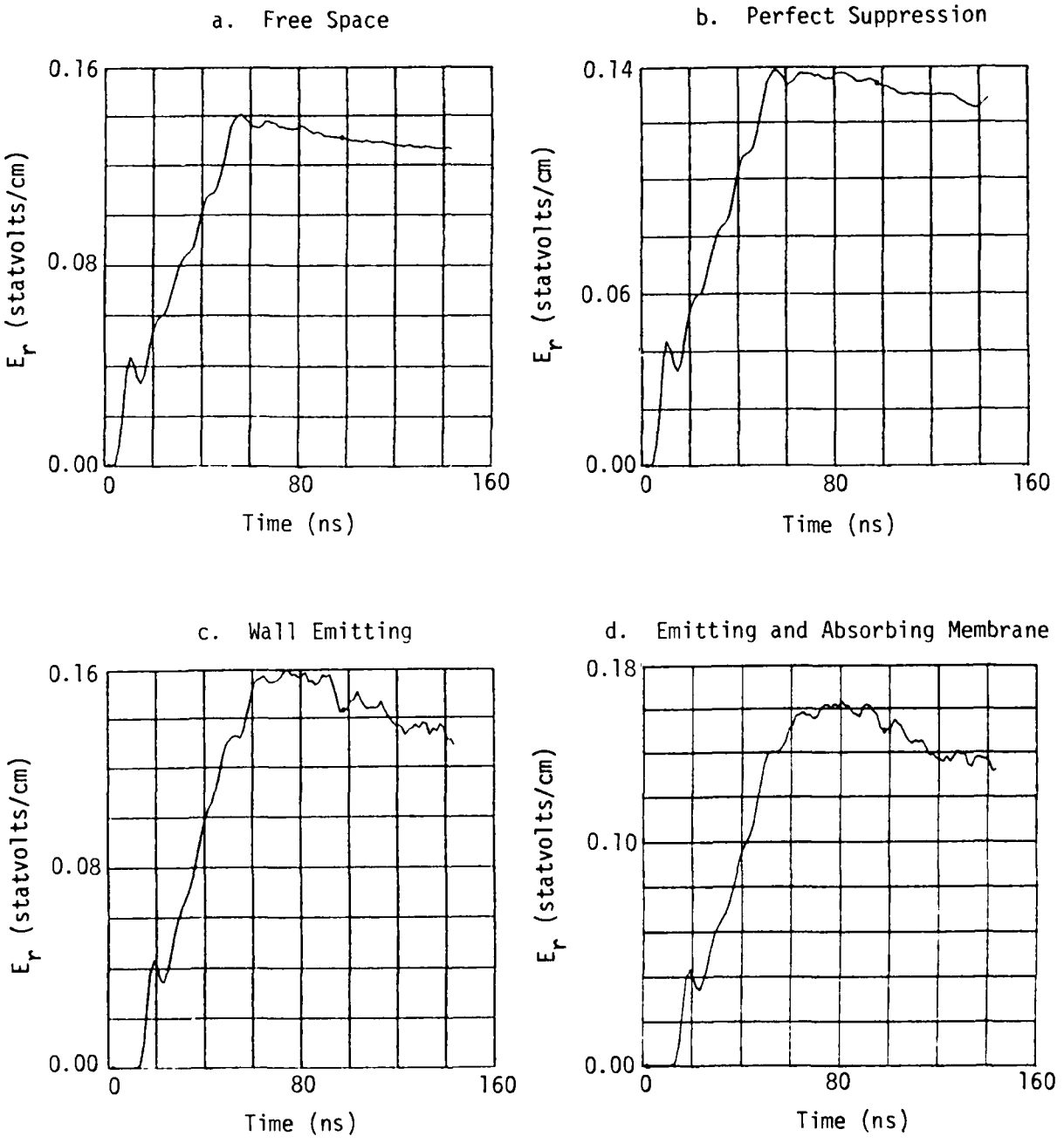


Figure 7. E-radial observer point 3 (unshifted).

A more dramatic demonstration of the consequences of reflection from the walls of the tank is observed at point 10. Figure 8 shows the behavior of $\int B^2 dt$ as a function of time at observer point 10 for the centered satellite cases. Here the general behavior of the fields is not dominated by the satellite emission as it was at point 3. In the plots shown in Figure 8, one can see clearly the signal reflected from the tank walls. At this point, the reflected pulse is actually larger than the initial pulse from the satellite. We point out that these curves do not show the total effect of the reflected pulse since the calculations were terminated at a time when the integral was still increasing rapidly (see Figures 8b, c and d).

Because of its distance from the emitting surface, the initial pulse deposits much less energy at observer point 10 than at observer point 3(two orders of magnitude less, see Figures 5a and 8a. In the perfect suppression case, the maximum value of the integral is an order of magnitude higher than in the free-space case. This increase is purely the result of reflection from the tank walls. Figure 8c indicates that the emission of electrons from the tank walls produces a further factor of 3 increase in the integral at late time $t > 100$ ns. Emission and absorption of electrons from the membrane has little additional effect on the energy deposited at observer point 10 (see Figures 5d and 8d).

From these results, we find that using the strawman design may cause differences of a factor of 30 in the integral of $B^2$ at observer point 10 (compare Figures 8a and 8c). Since the integral provides a measure of the Joule heating of the internal circuitry of the satellite, we must conclude that the influence of the tank walls may cause large increases in the amount of energy received at observer point 10. We may add that our estimate of a factor of 30 increase may be an underestimate since the calculations were terminated at a time when the value of the integral was increasing rapidly. A satellite placed inside a test tank could continue to extract energy from the cavity causing the energy received at certain points to exceed its free space value by a large factor.

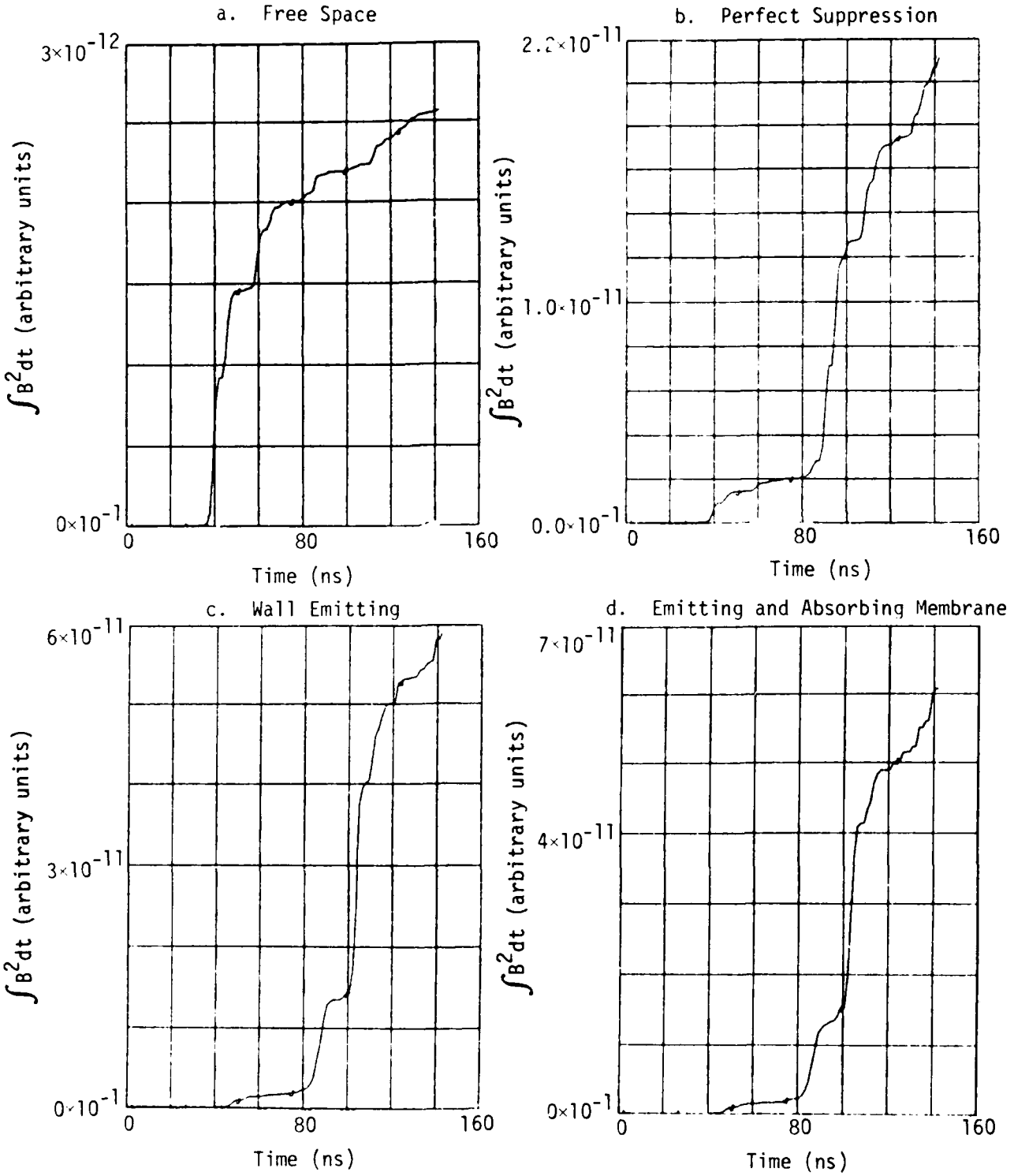


Figure 8. Integral of $B^2(t)$ observer point 10 (unshifted).

It is not clear that use of the strawman design for the SXTF would lead to overtesting of this type of satellite. Although point 10 receives much more energy in the strawman case than it does in the free-space case, the total amount of energy deposited at point 10 is much less than that deposited at point 3. Since a satellite must be able to withstand irradiation from any direction, this cannot be considered an overtest. However, at the particular observer point under discussion, this test fails to meet the criteria for simulation fidelity which requires that

$$1 \leq \frac{\int_0^\infty B_{sim}^2 dt}{\int_0^\infty B_{thr}^2 dt} \leq 3 ,$$

where the subscripts sim and thr refer to the simulation and threat sources respectively.[6] (We have substituted the free space response for the threat source in the above relation.)

We now consider the fields and currents produced at observer point 10. Figure 9 shows the behavior of the skin current at observer point 10 for all four cases. Here obvious differences are seen in the tank simulation cases as compared to the free-space case. The initial pulse at observer 10 is much smaller (by a factor of 10) than the initial pulse at observer point 3. While the initial pulse at point 10 is of the same size in all four cases, the reflection causes large differences to occur at late time. At this point, the reflected pulse is much larger than the initial pulse by a factor of 2 for the case of perfect suppression and a factor of 5 for the strawman case and for the case of the emitting membrane. Here the emission of electrons has a considerable effect on the amplitude of the reflected pulse.

From Figure 9 we see that at late time ($t \gtrsim 100$ ns), the magnitude of the skin current is one order of magnitude larger in the strawman case

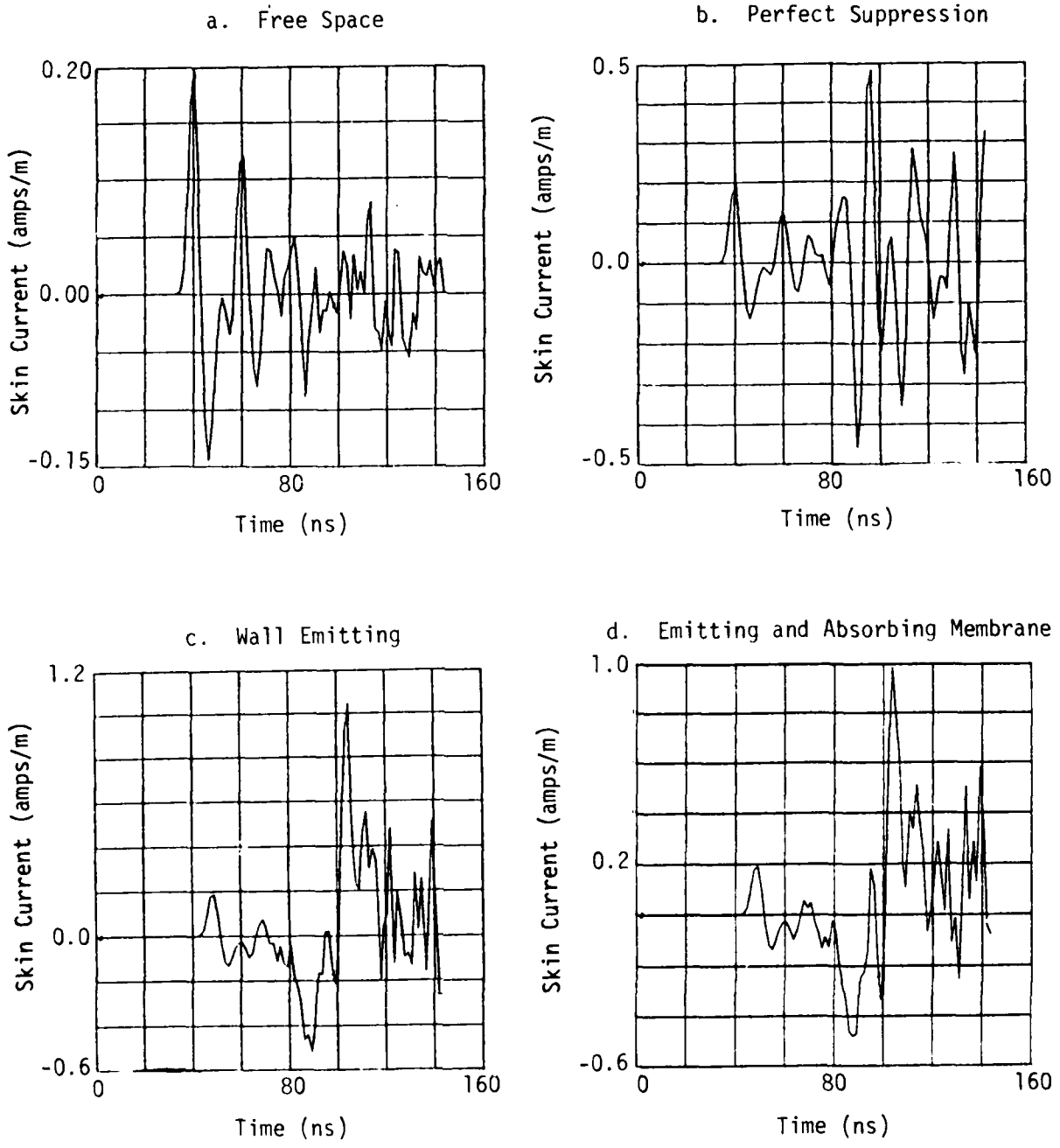


Figure 9. Skin current observer point 10 (unshifted).

than in the free-space case. However the skin current is still a factor of 3 lower than the current caused by the initial pulse at point 3 and as a result, we cannot consider that an overtest has occurred. The behavior of the skin current at late time is very different from the late time behavior of the skin current in the free-space case indicating that the simulation fidelity is poor at point 10.

Figure 10 shows the normal component of the electric field at observer point 10. Dramatic differences occur in the normal field for the strawman case. A large dip begins at the time when the wave is reflected from the walls of the tank. The $E_z$ component reaches a magnitude of approximately seven times greater than in the free-space case and has opposite sign. Furthermore, the overall shape of the curve is completely different. The initial rise is followed by a very deep minimum. Comparison of Figures 10c and 10d indicates that the emission and absorption of electrons from the *damper membrane* makes essentially no difference to the $E_z$ field at observer point 10. However, Figure 10c shows that the presence of emission from the tank walls causes an enhancement of the reflected signal. Evidence for this same effect can be seen in the skin current plots (Figure 9) although the effect here is not as pronounced as it is for the electric field.

The reason for this unexpected behavior is not fully understood but a possible mechanism is suggested in Section 4. The magnitude of the fields at point 10 is considerably less than the magnitude of the fields in the initial pulse at point 3 so that we cannot consider that an overtest has taken place. The fields differ from the free-space case to such an extent that the simulation quality criterion cannot be satisfied.

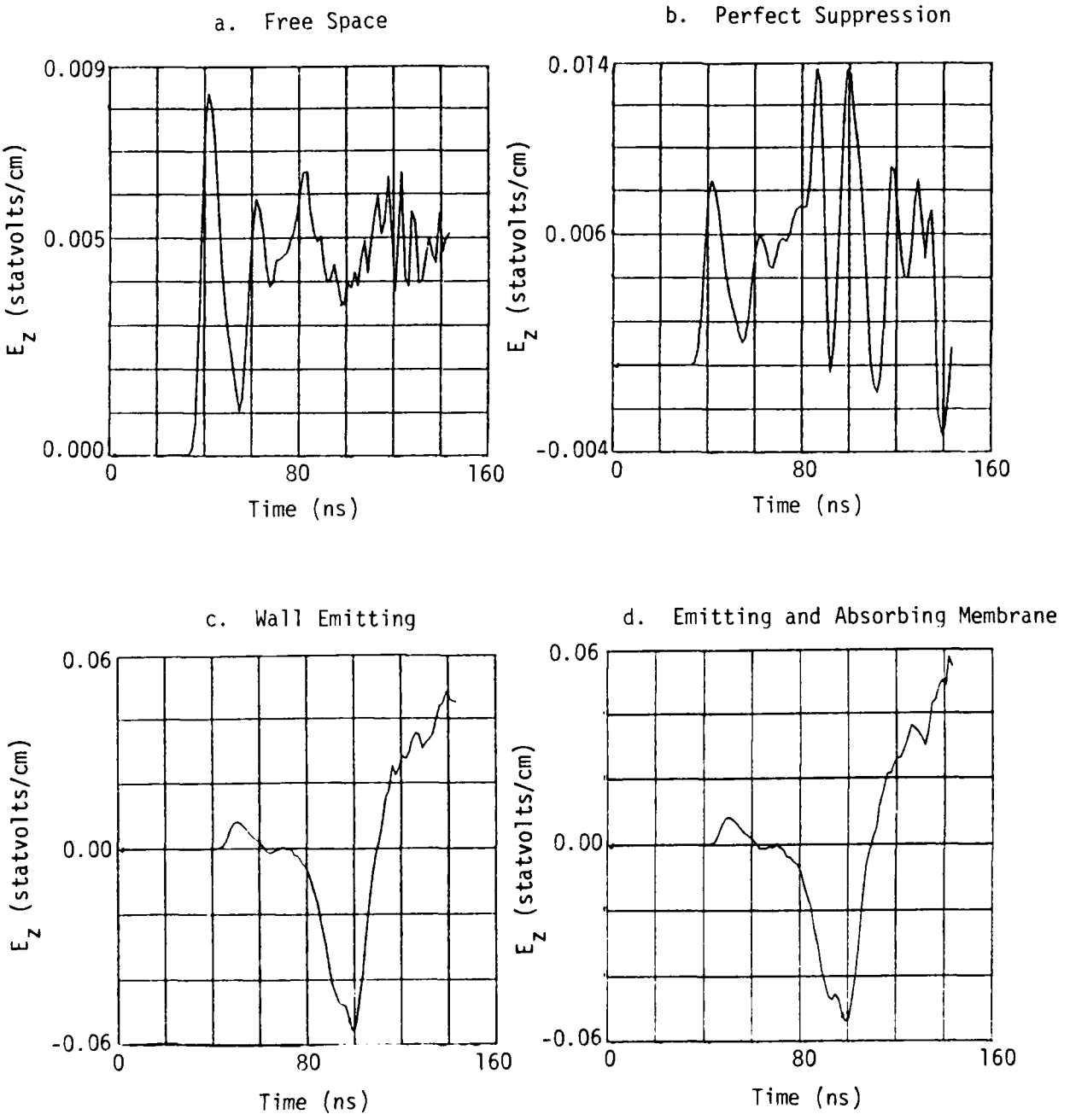


Figure 10. E-Z observer point 10 (unshifted).

## 3.5 SATELLITE OFF CENTER

A series of calculations was performed in which the satellite was removed from the center of the tank and placed close to the rear wall. In this configuration, the satellite was within 36 cm of the damper membrane. The purpose of these calculations was to examine the effects of having the satellite close to the tank walls. Stronger reflections are expected to occur in this case raising the possibility of overtesting. The satellite is now much closer to the source of electrons so that larger electric fields on the satellite may be produced. Considerations of the effects of the proximity of the satellite to the tank walls are of importance since it is probable that the SXTF will be used for tests of very large satellites whose dimensions will be comparable to those of the tank.

In order to examine in isolation the effects of position upon the reflection of electromagnetic waves, the fluence was not reduced from its value in the previous calculations. This assumption is not physically justified since the exploding wire radiation behaves as a spherical wave falling off as $1/r^2$.

The time integral of $B^2(t)$ at observer point 3 is shown in Figure 11. At observer point 3, the behavior of the integral is very similar to the behavior in the case of the centered satellite (Figure 5). Figure 11 indicates that in the case of the shifted satellite, the reflection from the tank walls deposits more energy on the satellite than it does in the case of the centered satellite but the difference is small (cf. Figures 5c and 11c). In the shifted satellite strawman case, the integral of $B^2(t)$ has a maximum value of only 10 percent higher than that attained in the centered satellite strawman case. From Figure 11d, we see that the emitting membrane has little effect on the overall behavior of the integral. At late time the value of the integral in the emitting membrane case is $\sim 10$ percent lower than in the strawman case (compare Figures 11c and 11d). This effect is similar to that seen in the centered satellite case (compare Figures 5c and 5d).

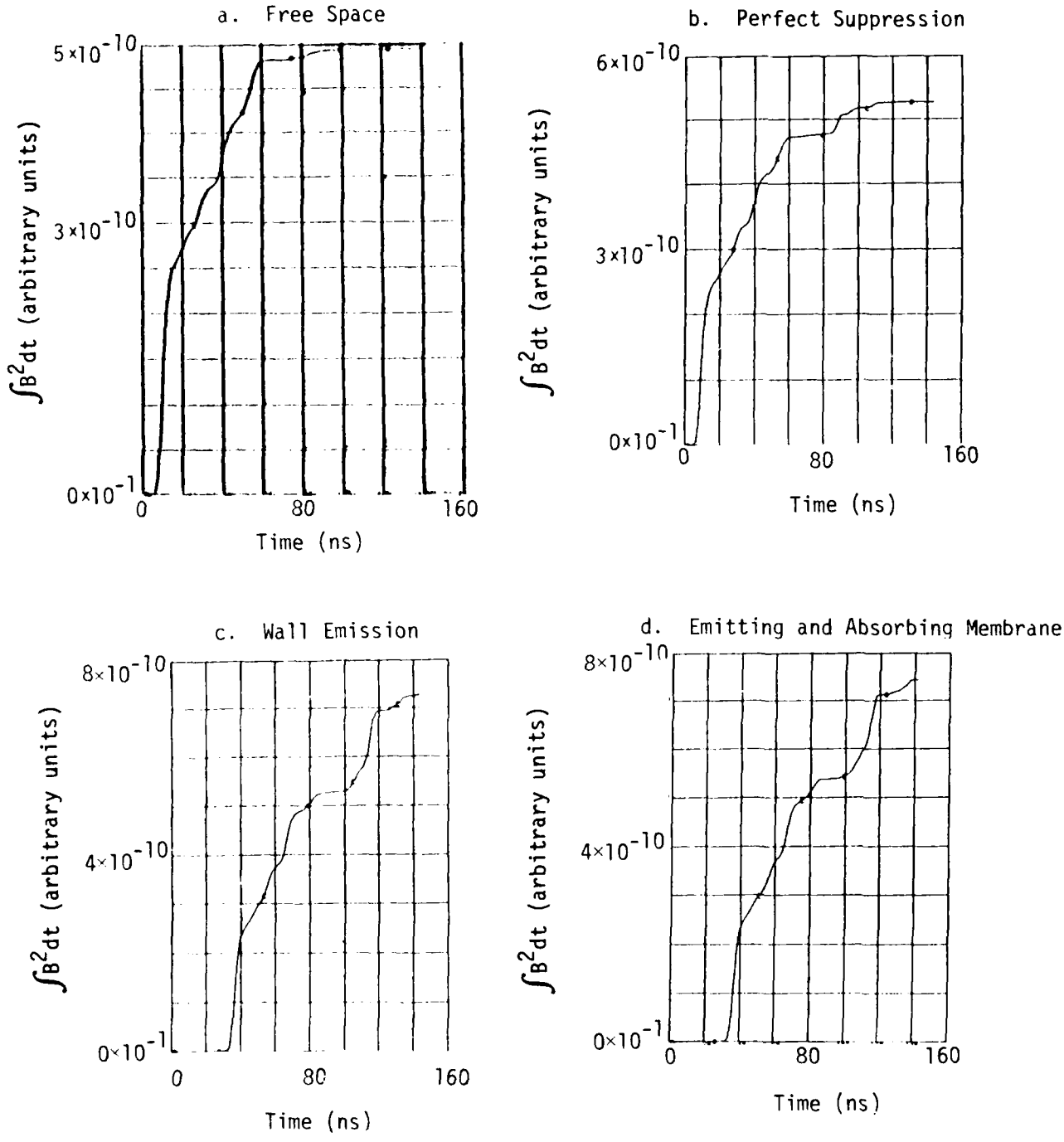


Figure 11. Integral of $B^2(t)$ observer point 3 (shifted).

From the plots in Figure 11, we see that the strawman case differs from the free-space case by less than a factor of 2 in $\int B^2(t)dt$. This close agreement between even the most extreme cases indicates that in the shifted satellite case, the simulation fidelity at observer point 3 is very good. Further evidence for the high quality of simulation is provided by the plots of skin current and normal component of the electric field shown in Figures 12 and 13 respectively.

The general behavior of the skin current is the same in all four cases; the sharp initial spike is followed by lower amplitude oscillations. In those cases in which the satellite is enclosed in the tank, the reflected pulse is quite prominent (Figures 12b, c and d) especially in those cases in which large quantities of electrons are present. In no case does the reflected pulse exceed $\sim 80$ percent of the initial pulse so that the skin current plots do not show any evidence for the possibility of overtesting. In addition, Figure 12 indicates that the reflected pulse never provides skin currents larger than twice the free space values (compare Figures 12a and 12c) so that the criteria for simulation fidelity are satisfied.

Comparison of the various cases shown in Figure 13 show that the behavior of the electric field is almost identical in all four cases. In summary we conclude that the influence of the tank walls do not give rise to overtesting and that the quality of the simulations at observer point 3 is very good.

The simulation fidelity is much worse at observer point 10. The plots of $\int B^2 dt$ for observer point 10 reveal that the strawman case differs from the free-space case by almost a factor of 200 (Figure 14). The presence of the tank in this case causes an enormous enhancement in the Joule heating of the circuitry at this point. However, the maximum value reached by the integral is still comparable to the value reached at point 3 in the free-space case so that although the simulation fidelity is very poor, no over-testing occurs.

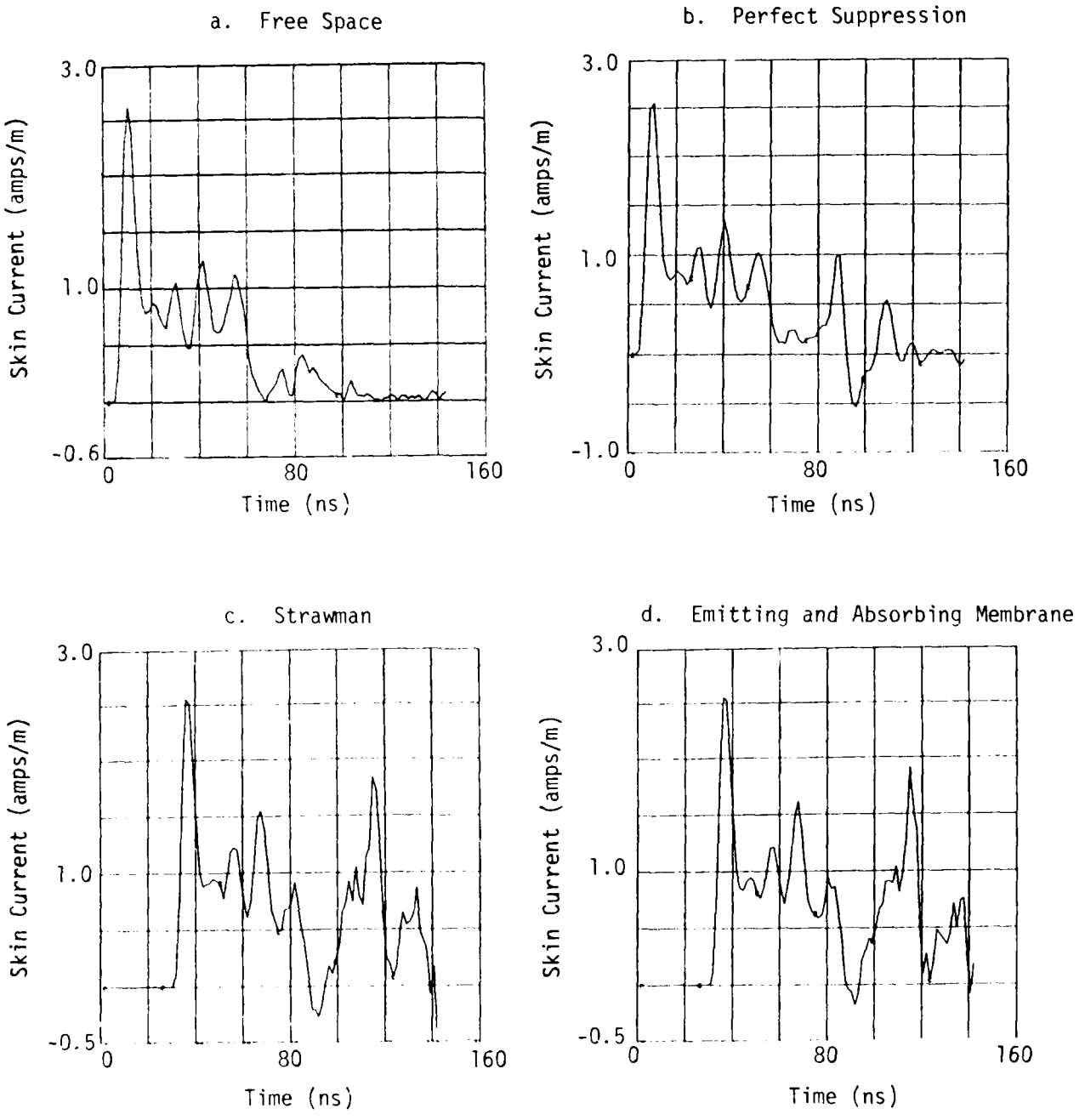


Figure 12. Skin current observer point 3 (shifted).

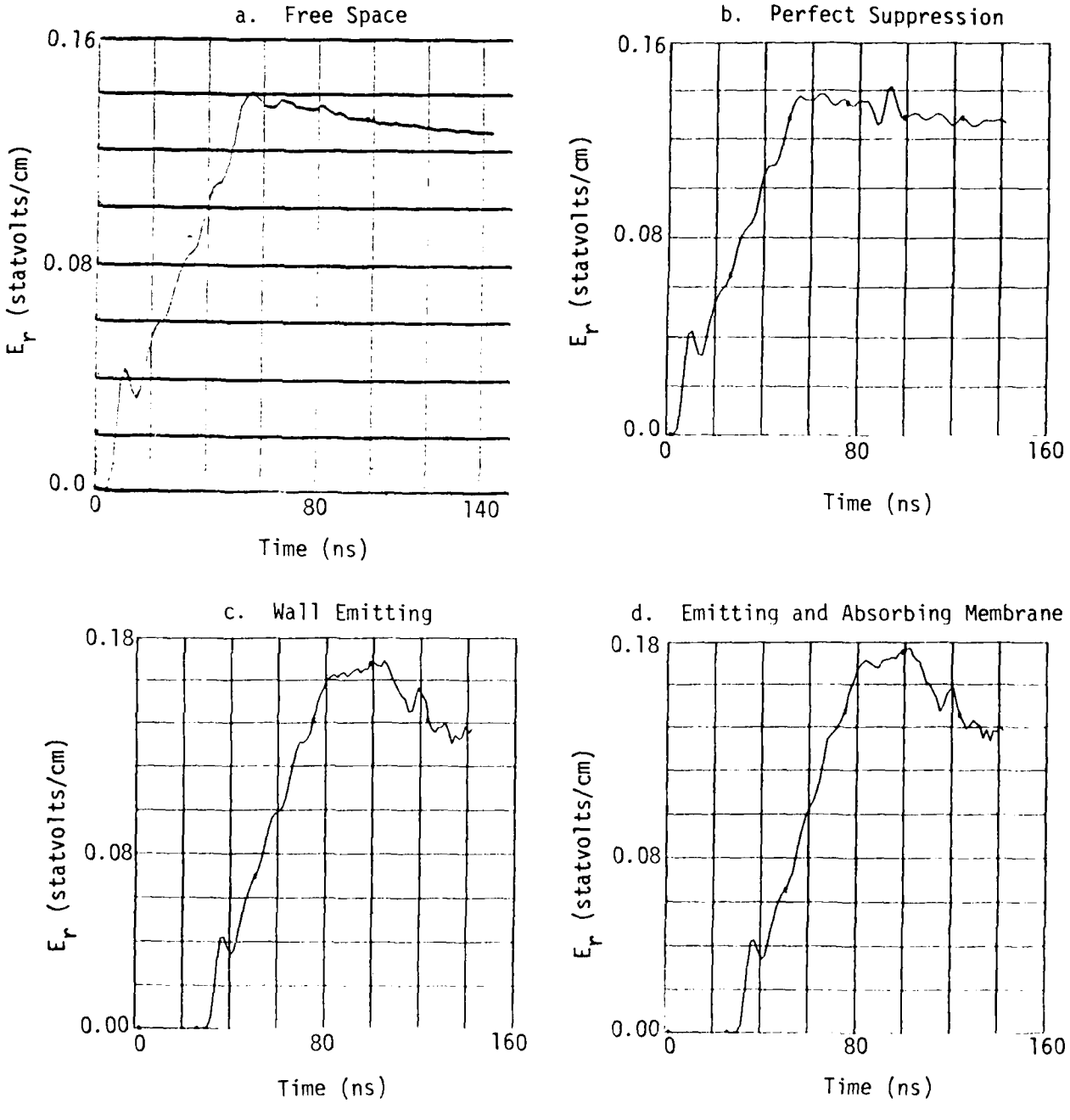


Figure 13. E-radial observer point 3 (shifted).

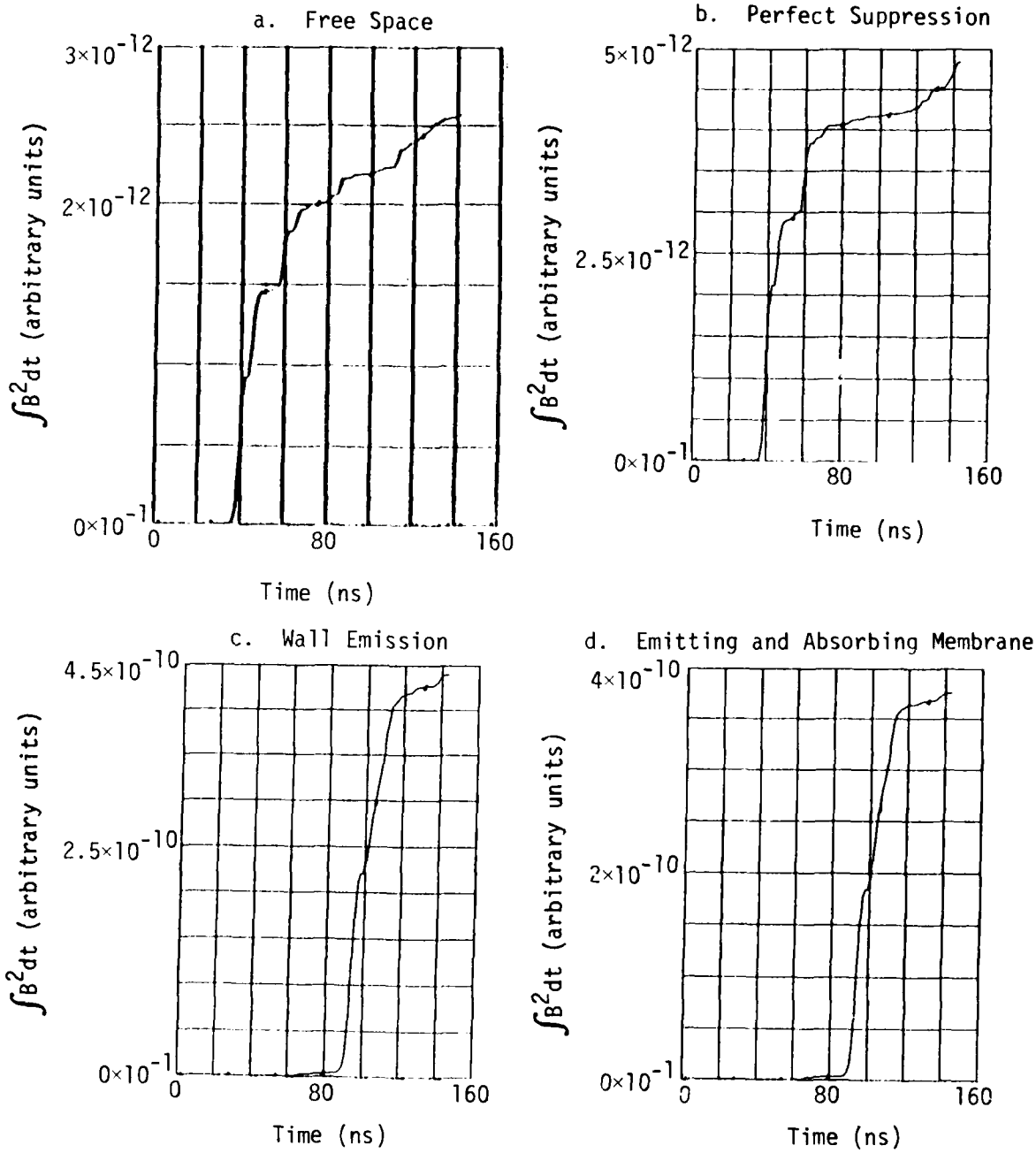


Figure 14. Integral of $B^2(t)$ observer point 10 (shifted).

There are large differences in the behavior of the skin current at observer point 10. The behavior of the skin current in the strawman and emitting membrane cases (Figures 15c, and 15d) differs from that of the free-space case in the same general way as they did in the centered satellite cases (Figures 9c and 9d) when the satellite is close to the tank walls, however, these differences are much more severe. The dip which occurs at the time of reflection $\sim 90$ ns is approximately an order of magnitude larger than the initial spike and has an opposite sign. These large differences in the behavior of the skin current are another indication of the poor quality of simulation at this point.

The reflected pulse in the perfect suppression case is much weaker in the shifted satellite case than it was in the centered satellite perfect suppression case (compare Figures 9b and 15b. This difference may be attributed to the proximity of the observer point to the damper membrane.

The most surprising results of this work are shown in Figure 16. Here we show the normal component of the electric field at observer point 10. $E_z$ reaches a magnitude of 20 times its free-space value and has an opposite sign in the strawman simulator. The magnitude of the field is comparable to that at observer 3 (see Figure 13). The behavior seen here is similar to but more extreme than that seen in the centered satellite case, with the field reaching a value of almost three times greater than that shown in Figure 10. After the dip, the field increases reaching positive values of over six times the free space maximum. At late time $t > 150$ ns, the strawman case behaves differently from either the free space or perfect suppression cases. Rather than oscillating about some positive mean (Figures 16a and 16b), the field decreases monotonically to very large negative values (-0.17 esu). We suggest that this decrease is caused by the deposition on the satellite of charge emitted from the tank walls. No significant differences were found in the behavior of the electric field at observer point 10 between the strawman case and the emitting membrane case.

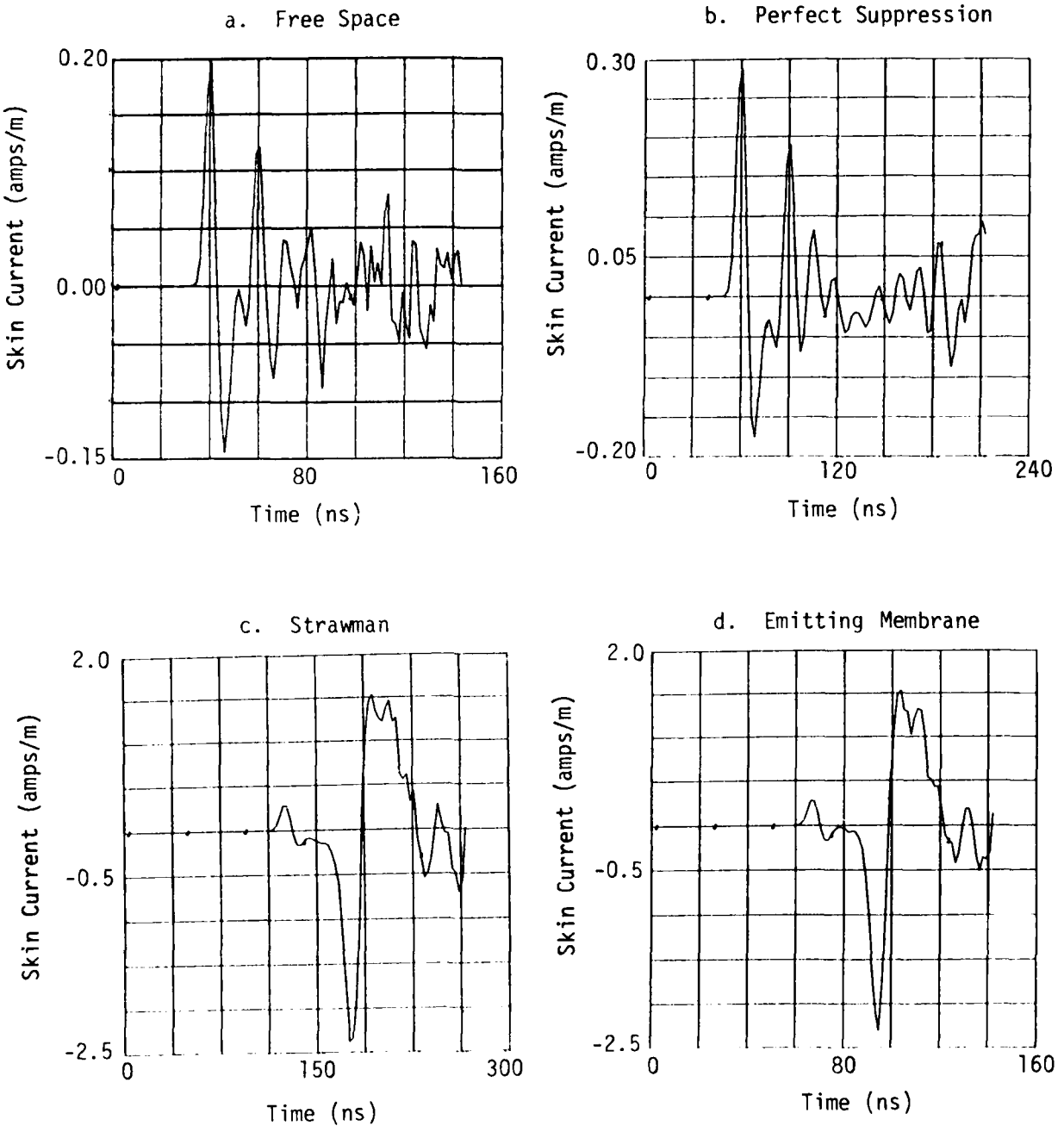


Figure 15. Skin current observer point 10 (shifted).

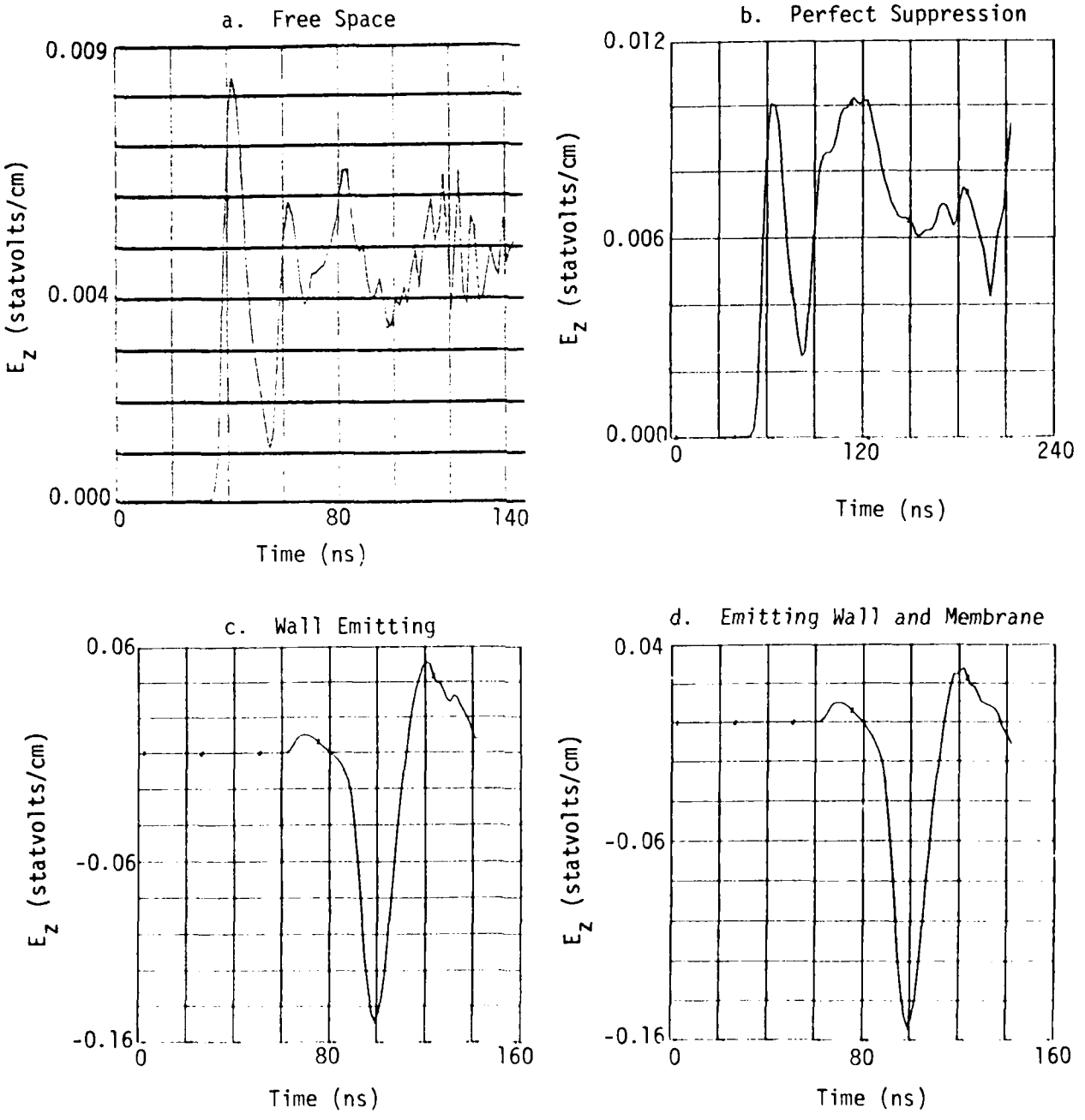


Figure 16. E-Z observer point 10 (shifted).

The surprising behavior of the fields at observer point 10 is not well understood and the next section of this report is largely concerned with our attempts to understand this phenomenon.

Finally, we may draw the following conclusions.

1. Simulation fidelity is generally very good at observer points close to the emitting surface of the satellite both for the perfect suppression case and for the strawman case. Fidelity is slightly worse when the satellite is positioned close to the tank walls but in all cases, the criteria for acceptable simulation fidelity are satisfied.

2. In no case was evidence for overtesting found. Although the fields produced at observer point 10 are much higher in the strawman case than they were in the perfect suppression case, they are never much greater than they are at observer point 3.

3. Since a satellite must be designed to survive irradiation from any direction we cannot consider this to be an overtest although the simulation fidelity is clearly unacceptable.

# SECTION 4
# ADDITIONAL CALCULATIONS

The peculiar behavior of the electric and magnetic fields described in the previous section is difficult to understand. Because of its implications for the SXTF design, we feel that it is important to be confident of these results and to develop some physical understanding. The calculations reported in this section were aimed primarily at determining the cause of the dip in the magnetic field shown in Figure 15 and in the electric field shown in Figure 16. Such factors as the amount of wall emission present, the X-ray spectrum, the X-ray emission time history and the method of calculating the movement of particles are examined. One purpose of these studies was to eliminate the possibility that the peculiar behavior of the fields is some artifact of the code. The details of the several cases examined are summarized in Table 2.

In Case A, the satellite is in the same position inside the tank as in the shifted satellite cases discussed in the previous section. Case A differs from the shifted satellite strawman case only in that electron emission occurs only from the front hemisphere of the tank and the damping membrane was removed. A significant difference in the results obtained in this case is that the normal component of the electric field at observer point 10 has decreased by approximately a factor of 2 (see Figure 17). The dip seen in the skin current in this case (Figure 18) is also smaller than that seen in the strawman case (Figure 15c). In addition, the oscillations in the fields do not damp out even at times as late as 600 ns. This lack of damping is due to the absence of the damper membrane. The reduction in the amplitude of the dip has two possible causes. Since the

Table 2. Summary of cases discussed in Section 4.

| Case | Satellite Present | Satellite Emitting | Sphere Emitting | Particles From Sphere | EW | Br | Retard |
|---|---|---|---|---|---|---|---|
| A | X | X | X | X | X | X | X |
| B | | | X | X | X | | X |
| C | | | X | X | | X | X |
| D | X | | X | | X | | X |
| E | | | X | | X | | |

EW - Exploding Wire

Br - Bremsstrahlung

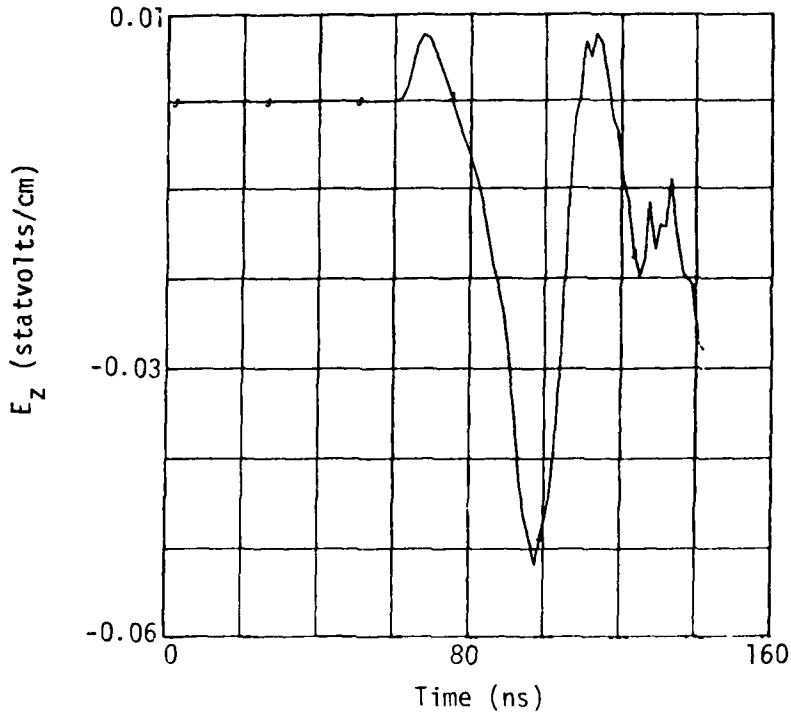


Figure 17. Case A—electric field at point 10.

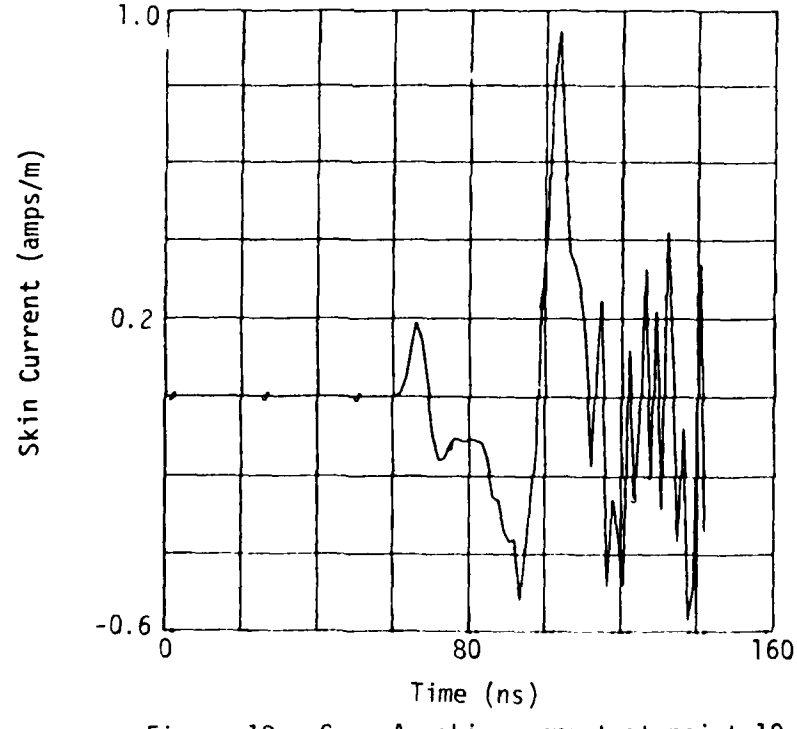


Figure 18. Case A—skin current at point 10.

differences between Case A and the strawman case are in the quantity and position of the emitted charge, we conclude that the reduction in the magnitude of the dip is attributable to one or other of these differences or to the combination of the two. This calculation suggests that the dip has its origin in the sphere rather than in the satellite.

We next examine the possibility that the peculiar behavior of the fields may in some way be caused by the presence of the satellite. Perhaps it is some artifact of the numerical algorithm of treating the thin current carrying struts. In order to rule out this type of possibility, we calculated Case B in which the satellite was removed from the tank and the sphere emission is only caused by the exploding wire X-ray source. The general behavior of the electric field in this case (shown in Figure 19) is similar to that found for Case A and to the shifted satellite strawman case shown in Figure 16c. The behavior of the skin current in Cases A and B are similar (Figure 20) with roughly the same magnitude of dip. The reflected magnetic field is approximately 40 percent stronger in Case B than in Case A where its maximum is 0.9 amp/m. The initial spike seen at $\sim 60$ ns in Figures 16c and 17 is caused by the interaction of the X-ray pulse with the satellite. Since no satellite is present in Case B, no initial spike is seen. The electric field at observer point 10 in Case B first departs from zero at $\sim 70$ ns due to the interaction of the X-ray pulse with the wall of the tank. A clear spike is produced reaching its greatest negative value at $\sim 95$ ns. The amplitude of this spike is reduced by a factor of four from the strawman case. The absence of the satellite reduced the amplitude of the spike but did not cause it to disappear. Although the presence of the satellite affects the size of the spike, it does not cause it. We can therefore exclude the possibility that the unexpected behavior of the fields is some artifact of our code description of the satellite. In addition, Case B clearly demonstrates that the dip is in some way caused by the sphere rather than the satellite.

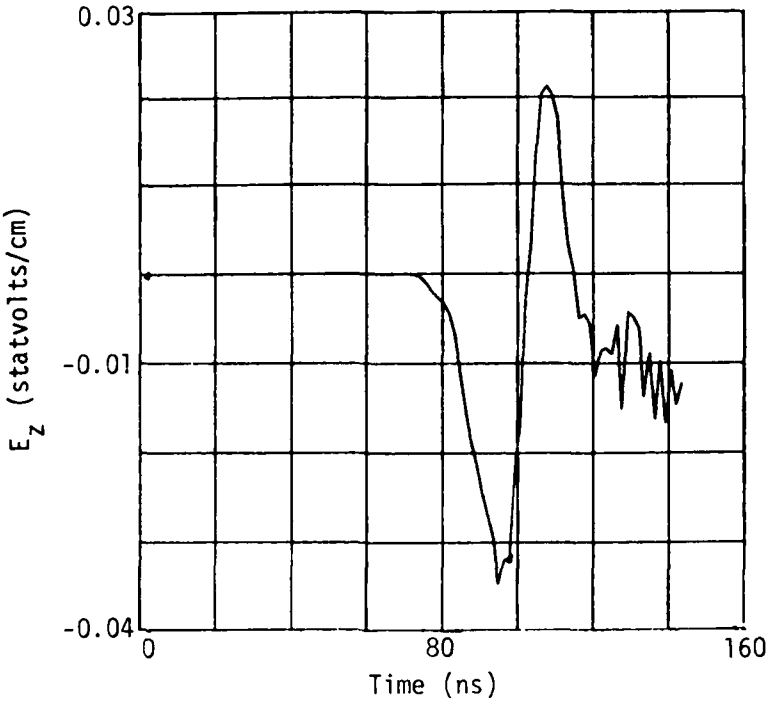


Figure 19. Case B—electric field at point 10.

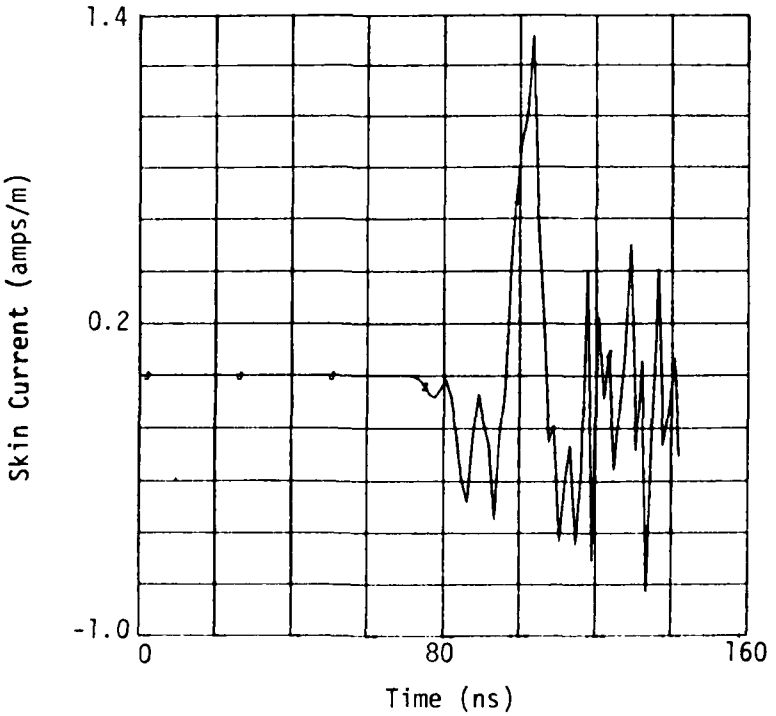


Figure 20. Case B—skin current at point 10.

In Case C we irradiate the sphere using the bremsstrahlung source only. The general behavior of the field (Figures 21 and 22) is remarkably similar to that seen in the strawman case and in Cases A and B described above. The magnitude of the dip is lower than in Case A by a factor of two and lower than the strawman case by a factor of five. We see that the dip is not strongly affected by the characteristics of the radiation striking the sphere.

In Cases D and E, we study the effect of retardation of the pulse. The radiation source is an exploding wire and particle emission is calculated using a dipole driver. The dipole driver is placed on the surface of the sphere and has the same magnitude and time history as that placed on the emitting surface of the satellite in Case A.

Case D resembles Case A in that we consider electron emission from the front half of the sphere and the satellite is present in the tank. Here, however, the emission from the satellite is neglected. The resulting curves are smoother due to the absence of noise caused by particle statistics. Figure 23 shows the behavior of the electric field in Case D. Because the dipole driver on the sphere has a large amplitude (appropriate in fact to the emitting surface of the satellite), a very strong dip occurs at the time of reflection. The dip is a factor of two larger than it is in the strawman case. Following the dip, the field rises to a very large positive peak (0.63 esu). The magnetic field at observer point 10 (Figure 24) initially behaves very much like the magnetic field in previous cases (e.g., A and B) but its behavior at late time is more extreme reaching a large positive peak and rapidly falling to a very large negative value. From case D we find that the presence of a non-emitting satellite has little effect on the dip. In addition, we are able to rule out the possibility that the dip is some artifact of our particle emitting and moving code.

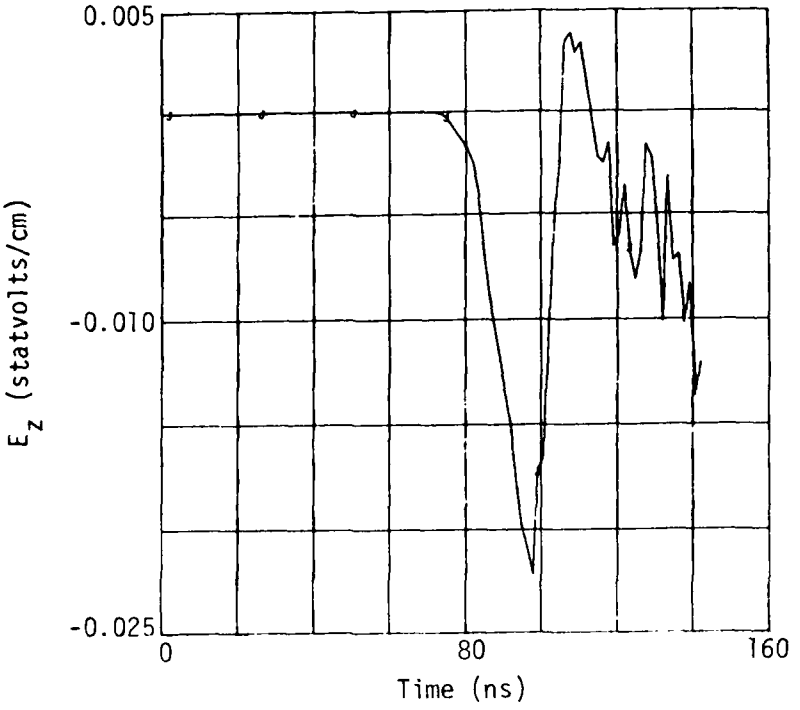


Figure 21. Case C—electric field at point 10.

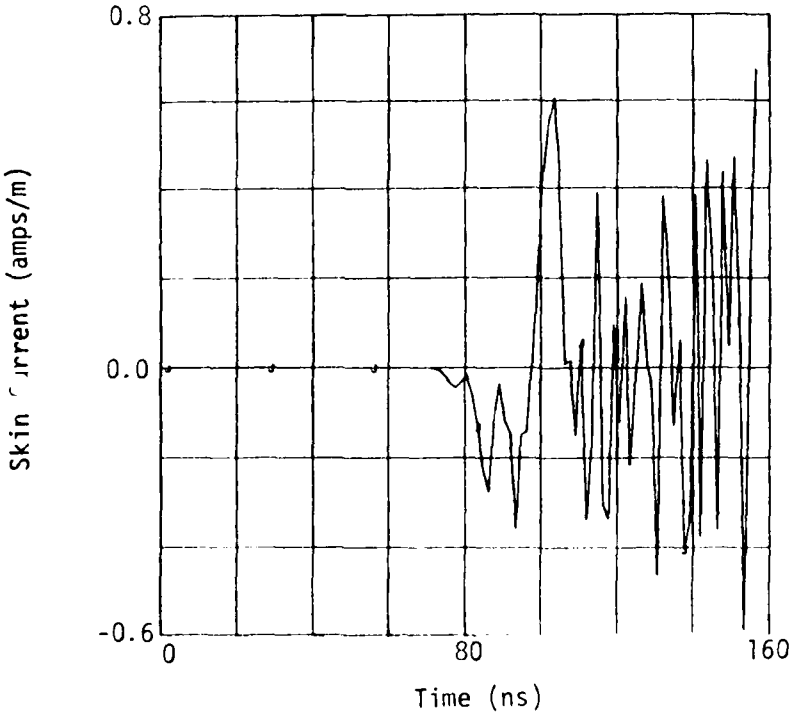


Figure 22. Case C—skin current at point 10.

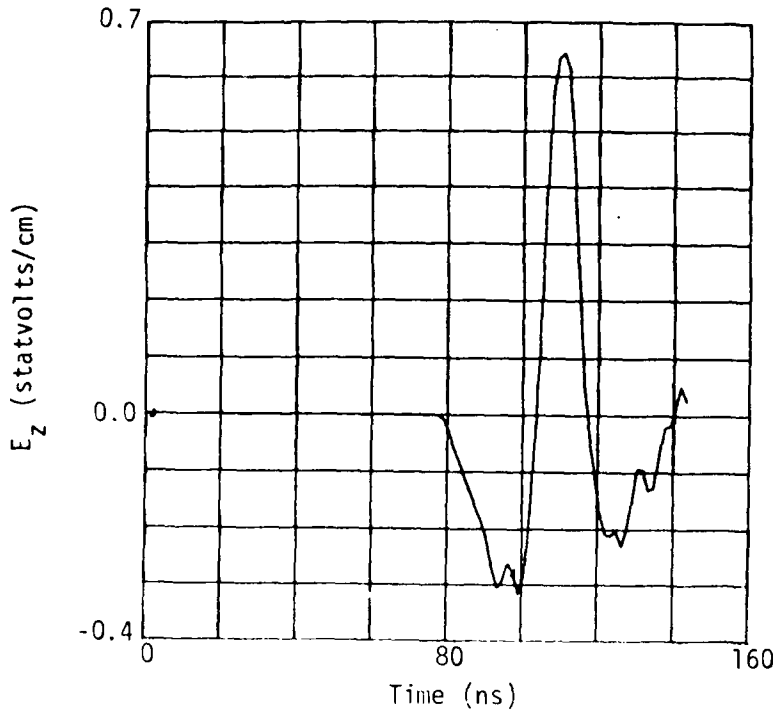


Figure 23. Case D—electric field at point 10.

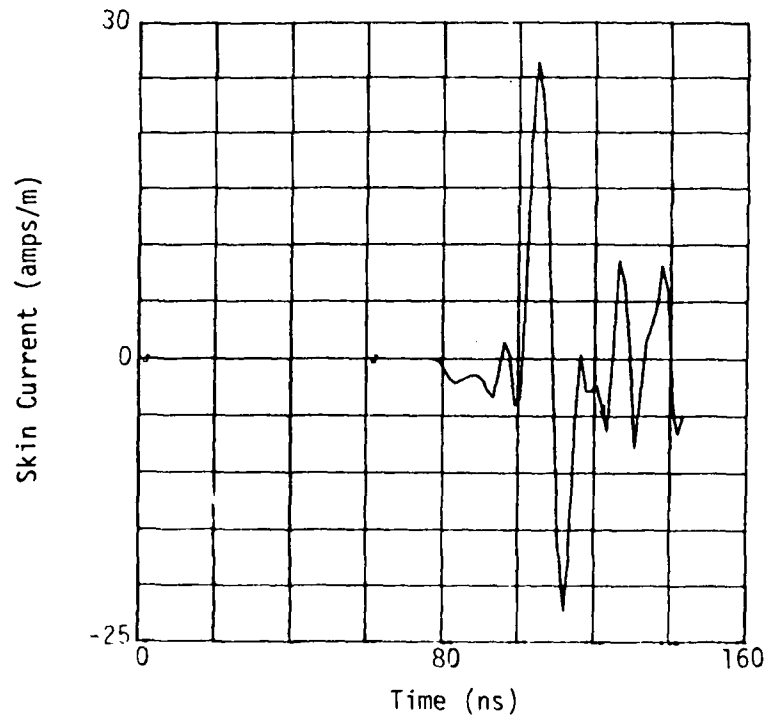


Figure 24. Case D—skin current at point 10.

In Case E, the satellite is absent and the emission from the sphere is from the exploding wire source only. Again we use the $\dot{P}$ description of the electron emission. In this case, the dipole driver is not retarded. Instead, the dipole layer forms simultaneously over the entire hemisphere. Comparison of Figure 25 and Figure 23 reveals that the dip in Case E is much less pronounced than in Case D. The unretarded dipole driver in Case E appears to have considerable influence on the behavior of the field. A local minimum occurs in $E_z$ at the time of reflection, but this seems to be simply the first in a series of oscillations. The magnetic field behaves similarly (Figure 26).

The phenomenon of the deep minimum is not completely understood. We have, however, ruled out several possibilities. This behavior has been shown not to be an artifact of our code description of the satellite, not an artifact of our particle emission algorithm or of our particle moving routines and is not caused (although it may be modified) by the presence of the satellite. The dip is not caused solely by either the exploding or bremsstrahlung emission. The dip appears to be directly related to the emission area on the sphere and is strongly influenced by the retardation of the emission of the sphere.

One possibility is that the dip arises from the excitation of a mode of the tank. The width of the dip in Case A is about 30 ns suggesting that a mode of frequency about 33 MHz may be excited. We wish to determine whether a mode of such a frequency can be excited by the dipole driver. In order to examine quantitatively the excitation of the sphere, we have calculated Case F. In this case we remove the satellite and excite the sphere using a truncated, unretarded driver. The dipole driver is the same as that used previously during the initial 13 ns and has zero magnitude thereafter. After 13 ns the undriven sphere rings and its modal response is shown on the Fourier spectrum of the magnetic field at the center of the mesh (Figure 27). Several harmonics are simultaneously excited. One of the strongest has a

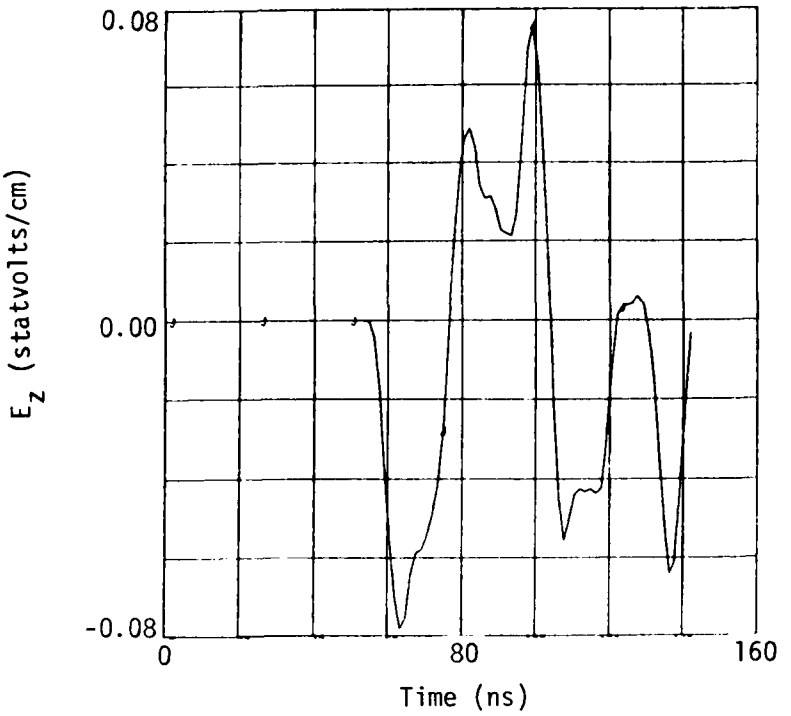


Figure 25. Case E—electric field at point 10.

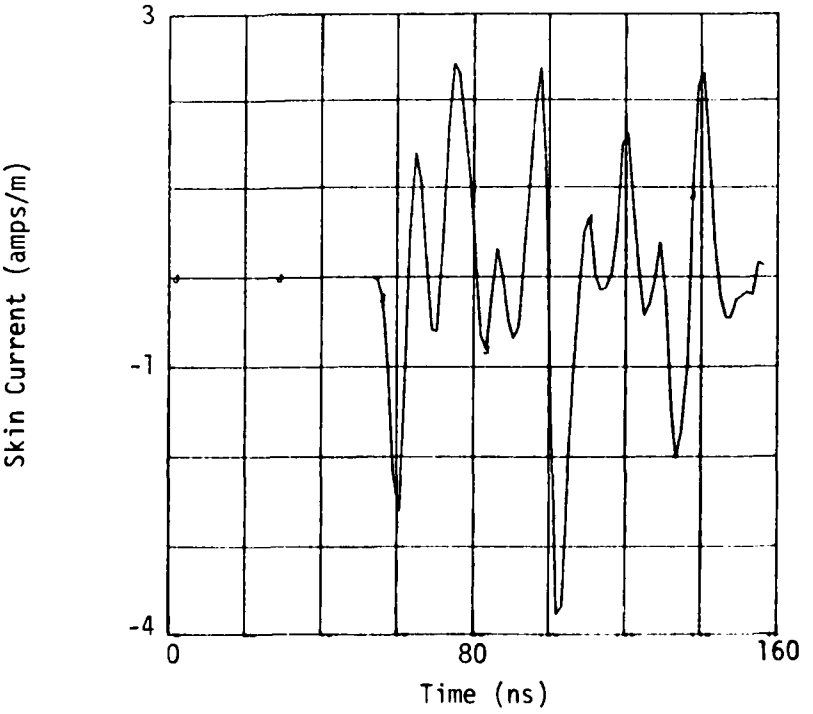


Figure 26. Case E—skin current at point 10.

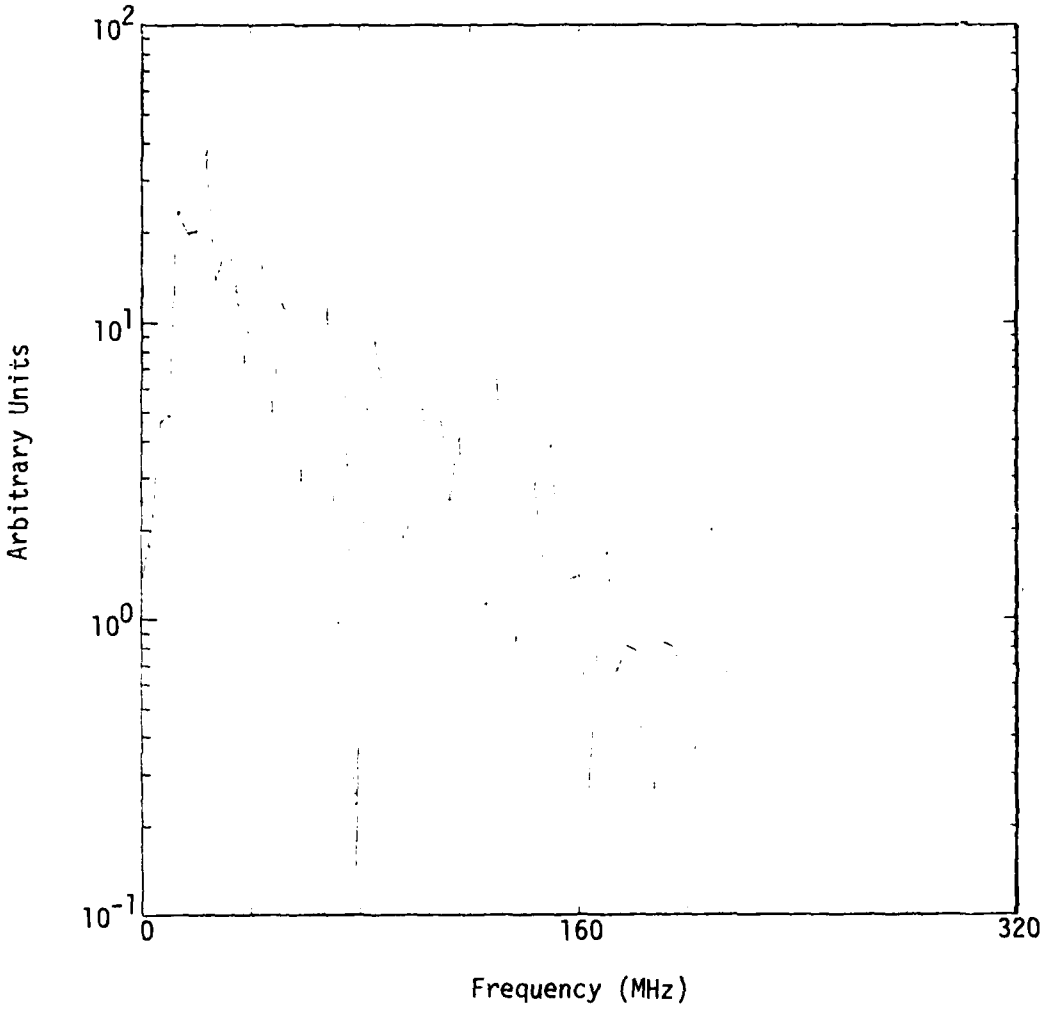


Figure 27. Fourier transform of magnetic field at center of mesh about 1000 cm from axis and 1200 cm from X-ray source.

frequency of 33 MHz suggesting that the spike may be the mode of the system having this frequency. The evidence for this is incomplete and many difficulties are encountered in trying to explain the behavior of the fields as excitations of modes of the sphere.

An alternative, perhaps more plausible, hypothesis for the cause of the dip will be detailed below.

Before describing the proposed hypothesis for the effect we will try to give some background for understanding the behavior of the EM fields in this system. The effect of a tank on an SGEMP simulation can be conveniently described in three successive parts. Prompt electromagnetic radiation effects caused by electron emission from a damper or tank walls arriving at the satellite at time, t, roughly equal to 2R/c, where R is the tank radius and c is the velocity of light (this time is 100 ns for the tank used in our simulation). Electromagnetic radiation effects caused by reflection from the tank walls can be described in terms of a modal picture. A modal description is most convenient after the radiation has assumed a global character which occurs after $t > 3R/c$ when one side of the tank has felt the presence of the other side. Before this time too many modes are necessary for an adequate description. The modal description is the second part of the system's behavior. The third part arises from electrons emitted by the walls, damper and source shields striking the satellite. Since electrons move slowly compared to the velocity of light and since the wall emission is to a first approximation spherically symmetric, the effect of electron impact can be described by electrostatics and occurs relatively late in time.

We suggest that the spike or dip effect is due to prompt electromagnetic radiation. Recurrence of the effect, should modes add up with the proper phasing, will be diminished due to the presence of the damper.

When photons arrive at the sphere walls electrons are emitted and slowed by the resulting electric fields. These circumstances give rise to both change of dipole moments and time rates of change of dipole moments at the wall. The magnetic field radiation from a dipole moment changing in time is given by

$$\vec{B} = \frac{1}{c^2} \frac{\hat{r} \times \dot{\vec{P}}}{r} \quad (\vec{E} = \vec{B} \times \hat{r}) \ ,$$

where $\vec{r}$ is the vector from the source to the field point and $\dot{\vec{P}}$ is in the radial direction. For this geometry the prompt magnetic field will be zero at the center of the tank and maximum near the edge where the effect of all the wall dipoles are additive. Therefore, the hypothesis compares qualitatively with the code calculation because the dip effect is greatest when the satellite is in the shifted position and decreases by a factor of two when only half the tank surface is illuminated or only half the wall dipoles exist.

Radiation from the dipoles do not arrive at the satellite simultaneously from all wall positions so the effect is spread out in time. For plane wave excitation the maximum time difference for waves arriving at the end of the spherical tank diametrically opposite the center of the source of the wave is 0.5 R/c. If all points on the wall are excited simultaneously the maximum time difference of arrival is 2R/c. We should therefore expect the ratio of the plane wave excited spike to the simultaneous wall emission to be in the ratio of 4 to 1. This seems again to be supported by the code computations. A characteristic magnitude for $\dot{P}$ from the 2 kV blackbody source is about $2 \times 10^{16}$ statamp/sec at the walls and lasting about 5 ns. We would therefore expect a prompt magnetic field arriving at 2R/c (100 ns) of duration about .5 R/c + 5 ns = 30 ns and having a magnitude of about

$$\frac{1}{2} \frac{1}{c^2} \frac{\ddot{P}}{R} 4\pi R^2 \left(\frac{5}{30}\right) = .035 \text{ gauss} \cong 3 \text{ amp/m} \ .$$

The 1/2 in the above calculation arises because the average of $\hat{r} \times \dot{\vec{P}}$ is estimated as 1/2; the factor of 5/30 arises because the $\dot{P}$ pulse is about 5 ns but is spread over 30 ns. The estimated character of the prompt pulse agrees with the observed character in Figure 15 and supports the proposed hypothesis for the dip effect.

# SECTION 5
# RECOMMENDATIONS

The presence of the tank and electron emission from the walls do not appear to affect the fields on and near the satellite in such a way as to cause severe overtesting. Even in our most extreme case Figure 16c, the magnitude of the field produced at observer 10 is approximately the same as that seen at observer 3. Our results indicate, however, that while acceptable simulation is produced in the perfect suppression case, the more realistic case of an emitting tank wall produces very poor simulation fidelity at specific points. The departure of the response from the free-space response is most severe when the satellite is placed close to the tank walls, indicating that for a strawman design SXTF, serious fidelity problems may arise in tests of larger satellites.

Suppression of electron emission from the tank walls appear to be required to remedy this situation. Coating the tank walls with carbon (a low-photoelectric yield substance) as in the strawman design is inadequate. Additional suppression or collimation is necessary. If collimation is not sufficient, an active suppression grid maintained at a fixed potential may be necessary in order to prevent wall electrons from causing a large tank response.

## REFERENCES


1. Wenaas, E. P., R. H. Stahl, and R. M. Wheeler, SXTF Strawman Facility Design RDT&E Portion Details, RE-78-2066-077, Jaycor, July 1978.

2. Stettner, R., Generalized Boundary Condition in SEMP, MRC-R-196, DNA 3999T, Mission Research Corporation, October 1975.

3. Carron, N. J., Description of the Code SCAL1D for Calculating the One-Dimensional SGEMP Boundary Layer, MRC-R-267, DNA 4237T, Mission Research Corporation, May 1976.

4. Goldstein, B., A Membrane Damping System for a Small SGEMP Simulator Chamber, MRC-R-388, Mission Research Corporation, April 1978.

5. Stettner, R., and R. Marks, A Non-Reflecting Electromagnetic Outer Boundary Condition for Cylindrical Coordinates and the SGEMP Problem, MRC-R-194, Mission Research Corporation, June 1975.

6. Carron, N. J., C. Rathmann, V. van Lint, and L. Cotter, Satellite X-ray Test Facility Technical Study, MRC-R-372, Mission Research Corporation, July 1978.

7. Parks, D., J. Gilbert, and I. Katz, A Technique for Treating Small Current Carrying Struts in Electromagnetic Particle Pushing Codes, SSS-R-76-2847, Science, Systems and Software, January 1976.

8. Lee, K. M., Thin Wire Approximation in 2-D Finite Difference Calculation of EMP Response, AMRC-N-96, Mission Research Corporation, August 1978.

# APPENDIX A
# TREATMENT OF THIN CURRENT CARRYING STRUTS

Our calculations attempt to describe electromagnetic phenomena inside a tank of radius 30 m. The test body consists of three cylinders connected by struts of radius 1.25 cm. Clearly it is not possible to use a mesh fine enough to describe the struts while at the same time covering the entire space of interest. Such a description of the problem would require enormous amounts of computer storage and CP time. An alternative procedure is required.

Our technique of treating thin struts is similar to that described by Parks, et al.[7] and Lee.[8] We shall present a brief outline of this method.

In general, Faraday's equation may be written

$$\underset{\sim}{\nabla} \times \underset{\sim}{E} = - \frac{1}{c} \frac{\partial B}{\partial t} .$$

Integrating the equation and making use of Stoke's theorem, we obtain

$$\frac{1}{c} \int \frac{\partial B}{\partial t} \cdot da = - \oint \underset{\sim}{E} \cdot d\underset{\sim}{\ell}$$

Now consider this equation as it applies to some cell lying on the Z axis and consider a thin conducting strut of radius $a << \Delta r$ lying along the Z axis. Faraday's equation may then be integrated with the area of integration being the shaded area in Figure A-1 and the contour being its perimeter.

Using the fact that the field in the vicinity of the strut varies like 1/r, the surface integral becomes

$$\frac{\Delta Z}{c}\int_{a}^{\Delta r/2}\frac{\partial B(a)}{\partial t}\left(\frac{a}{r}\right)dr \ .$$

Carrying out the integration we have

$$\frac{\Delta Z}{c}\frac{\partial B(a)}{\partial t}\, a\ell n(\Delta r/2a) \ .$$

The line integral becomes, since $E_z$ vanishes on the conductor and the normal field to a cylindrical conductor varies as 1/r

$$-E_{z_1}\Delta Z + E(a)_{r,\ell+1}\int_{a}^{\Delta r/2}\frac{a}{r}\,dr - E(a)_{r,\ell}\int_{a}^{\Delta r/2}\frac{a}{r}\,dr$$

$$= -E_{z_1}\Delta Z + (E(a)_{r,\ell+1} - E(a)_{r,\ell})a\ell n\ (\frac{\Delta r}{2a}) \ .$$

Rearranging the terms, the integrated Faraday equation becomes

$$\frac{\partial B(a)}{\partial t} = c\,\frac{E_{z_1}}{a\ell n(\Delta r/2a)} - c\,\frac{E(a)_{r,\ell+1} - E(a)_{r,\ell}}{\Delta Z} \ .$$

This equation differs from the usual difference formulation of Faraday's equation only in that the term in $E_{z_1}$ has been added.

Ampere's equation may be treated similarly. In general, we have

$$\frac{1}{c}\frac{\partial \underset{\sim}{E}}{\partial t} = \underset{\sim}{\nabla} \times \underset{\sim}{H} - 4\pi\,\underset{\sim}{J} \ ,$$

where J is in abamperes per $cm^2$. Integrating and making use of Stoke's theorem

$$\frac{1}{c}\int\frac{\partial \underset{\sim}{E}}{\partial t}\cdot d\underset{\sim}{a} = \oint \underset{\sim}{H}\cdot d\underset{\sim}{\ell} - 4\pi\int\underset{\sim}{J}\cdot d\underset{\sim}{a} \ ,$$

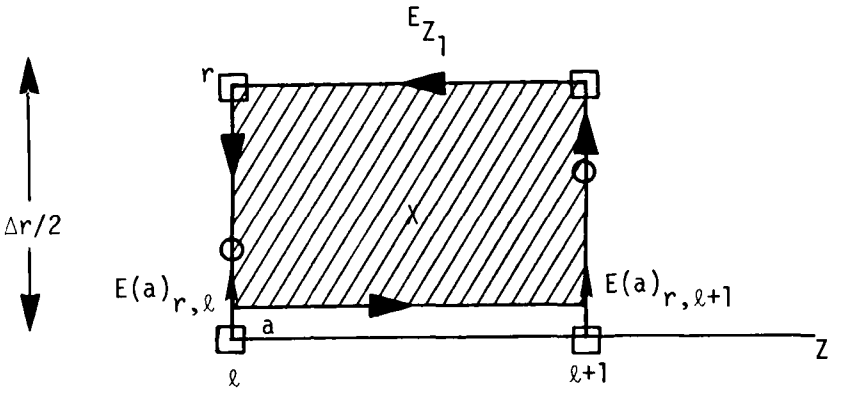


Figure A-1. Wire lying along Z axis with a << $\Delta r$. Contour of integration for $\underset{\sim}{E}$.

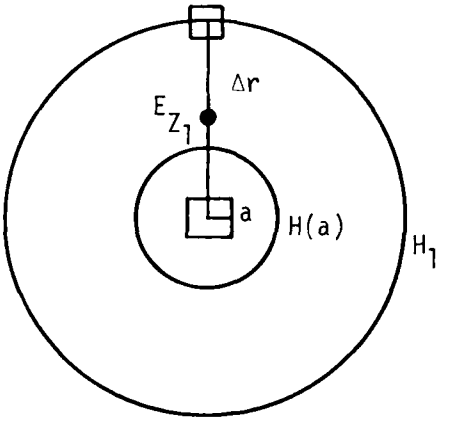


Figure A-2. Contour of integration for H.

where the area of integration is the circle of radius $\Delta r$ (see Figure A-2) and the contour of integration is the circumference of the circle. Then neglecting the small area of the wire

$$\frac{\pi \Delta r^2}{c} \frac{\partial E_{-1}}{\partial t} = 2\pi \Delta r H_1 - 2\pi a H(a) \ ,$$

which becomes, on rearranging

$$\frac{\partial E_{-1}}{\partial t} = \frac{2c}{\Delta r} H_1 - \frac{2ac}{\Delta r^2} H(a) \ ,$$

which is simply the usual difference formulation of Ampere's equation with an additional term.

The radial component of Ampere's law is

$$\frac{1}{c} \frac{\partial E_r}{\partial t} = [\nabla \times H - 4\pi J]_r \ .$$

Integrating over the surface of the wire furnishes an equation relating the normal electric field and the surface magnetic field.

These modifications of Maxwell's equations permit the calculation of the fields in the vicinity of the wire and makes possible an accurate description of the electromagnetic behavior of the test body using a mesh large compared to the strut radius. One can thus realize large savings in computer storage and CP time.

# DISTRIBUTION LIST

DEPARTMENT OF DEFENSE

Assistant to the Secretary of Defense
Atomic Energy
ATTN: Executive Assistant

Defense Intelligence Agency
ATTN: DB-4C

Defense Nuclear Agency
2 cy ATTN: RAEV
4 cy ATTN: TITL

Defense Technical Information Center
12 cy ATTN: DD

Field Command
Defense Nuclear Agency
ATTN: FCLMC
ATTN: FCPR

Field Command
Defense Nuclear Agency
Livermore Branch
ATTN: FCPRL

Interservice Nuclear Weapons School
ATTN: TTV

Joint Chiefs of Staff
ATTN: J-5 Nuclear Division
ATTN: C3S Evaluation Office

Joint Strat Tgt Planning Staff
ATTN: JLA
ATTN: JLTW-2

National Communications System
ATTN: NCS-TS

Undersecretary of Def for Rsch & Engrg
ATTN: Strategic & Space Sys (OS)
ATTN: AE

DEPARTMENT OF THE ARMY

BMD Advanced Technology Center
Department of the Army
ATTN: ATC-O

BMD Systems Command
Department of the Army
ATTN: BDMSC-H

Deputy Chief of Staff for Rsch Dev & Acq
Department of the Army
ATTN: DAMA-CSS-N

Electronics Tech & Devices Lab
U.S. Army Electronics R&D Command
ATTN: DRSEL

Harry Diamond Laboratories
Department of the Army
ATTN: DELHD-N-RBC, R. Gilbert
ATTN: DELHD-I-TL

DEPARTMENT OF THE ARMY (Continued)

U.S. Army Communications Sys Agency
ATTN: CCM-AD-LB

U.S. Army Foreign Science & Tech Ctr
ATTN: DRXST-IS-1

U.S. Army Missile R&D Command
ATTN: RSIC

DEPARTMENT OF THE NAVY

Naval Research Laboratory
ATTN: Code 6707, K. Whitney
ATTN: Code 7550, J. Davis
ATTN: Code 6701

Naval Surface Weapons Center
ATTN: Code F31

Strategic Systems Project Office
Department of the Navy
ATTN: NSP

DEPARTMENT OF THE AIR FORCE

Air Force Geophysics Laboratory
ATTN: PH, C. Pike

Air Force Weapons Laboratory
Air Force Systems Command
ATTN: SUL
ATTN: NT
ATTN: NXS
2 cy ATTN: DYC

Ballistic Missile Office
Air Force Systems Command
ATTN: MNNH
ATTN: MNRTE
ATTN: MNNG

Deputy Chief of Staff
Research, Development, & Acq
Department of the Air Force
ATTN: AFRDQI

Headquarters Space Division
Air Force Systems Command
ATTN: SKF

Rome Air Development Center
Air Force Systems Command
ATTN: ESR, E. Burke

Strategic Air Command
Department of the Air Force
ATTN: NRI-STINFO Library
ATTN: XPFS

OTHER GOVERNMENT AGENCIES

Central Intelligence Agency
ATTN: OSWR/STD/MTB, A. Padgett

OTHER GOVERNMENT AGENCIES (Continued)

NASA
ATTN: N. Stevens
ATTN: C. Purvis
ATTN: Library

DEPARTMENT OF ENERGY CONTRACTORS

Lawrence Livermore National Laboratory
ATTN: Technical Information Dept Library

Los Alamos National Scientific Laboratory
ATTN: MS 364

Sandia National Laboratories
Livermore National Laboratory
ATTN: T. Dellin

Sandia National Laboratories
ATTN: Code 3141

DEPARTMENT OF DEFENSE CONTRACTORS

Aerospace Corp
ATTN: Library
ATTN: V. Josephson

AVCO Research & Systems Group
ATTN: Library A830

Boeing Co
ATTN: P. Geren

Computer Sciences Corp
ATTN: A. Schiff

Dikewood Industries, Inc
ATTN: Technical Library

Dikewood Industries, Inc
ATTN: K. Lee

EG&G Washington Analytical Services Center, Inc
ATTN: Library

Ford Aerospace & Communications Corp
ATTN: A. Lewis
ATTN: Technical Library

General Electric Co
ATTN: J. Peden

General Electric Company—TEMPO
ATTN: W. McNamara
ATTN: DASIAC

Hughes Aircraft Co
ATTN: Technical Library

Hughes Aircraft Co
ATTN: E. Smith
ATTN: W. Scott
ATTN: A. Narevsky

Institute for Defense Analyses
ATTN: Classified Library

TRW Defense & Space Sys Group
ATTN: D. Clement
ATTN: Technical Information Center

DEPARTMENT OF DEFENSE CONTRACTORS (Continued)

IRT Corp
ATTN: B. Williams
ATTN: Library
ATTN: N. Rudie

JAYCOR
ATTN: E. Wenaas
ATTN: Library

JAYCOR
ATTN: R. Sullivan

Johns Hopkins University
ATTN: P. Partridge

Kaman Sciences Corp
ATTN: W. Rich
ATTN: Library
ATTN: N. Beauchamp
ATTN: D. Osborn

Lockheed Missiles & Space Co, Inc
ATTN: Dept 85-85

McDonnell Douglas Corp
ATTN: S. Schneider

Mission Research Corp
ATTN: C. Longmire
ATTN: R. Stettnner
5 cy ATTN: Document Control

Mission Research Corp
ATTN: B. Goplen

Mission Research Corp—San Diego
ATTN: V. Van Lint
ATTN: Library

Pacific-Sierra Research Corp
ATTN: H. Brode

R & D Associates
ATTN: S. Siegel
ATTN: Technical Information Center
ATTN: L. Schlessinger
ATTN: R. Schaefer
ATTN: P. Haas

Rockwell International Corp
ATTN: Library

Science Applications, Inc
ATTN: W. Chadsey

Spire Corp
ATTN: R. Little

SRI International
ATTN: Library

Systems, Science & Software, Inc
ATTN: A. Wilson
ATTN: Library

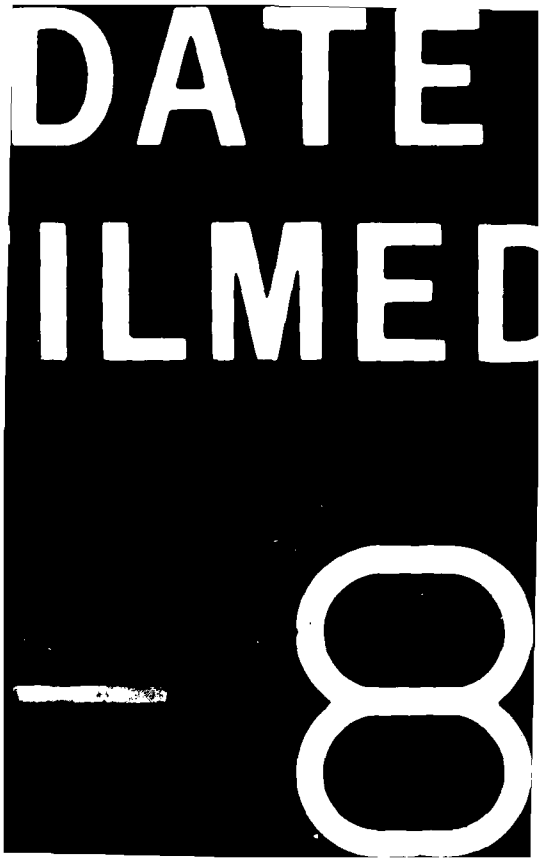
DATE
ILMED
8